2004-03-17

Active Minimization of Acoustic Energy Density in a Mock Tractor Cab

Benjamin Mahonri Faber
Brigham Young University - Provo

ACTIVE MINIMIZATION OF ACOUSTIC ENERGY DENSITY IN A MOCK TRACTOR CAB

by

Benjamin M. Faber

A thesis submitted to the faculty of

Brigham Young University

in partial fulfillment of the requirements for the degree of

Master of Science

Department of Physics and Astronomy

Brigham Young University

April 2004

BRIGHAM YOUNG UNIVERSITY

GRADUATE COMMITTEE APPROVAL

of a thesis submitted by

Benjamin M. Faber

This thesis has been read by each member of the following graduate committee and by majority vote has been found to be satisfactory.

Date	Scott D. Sommerfeldt, Chair
Date	Timothy W. Leishman
Date	Jonathan D. Blotter

BRIGHAM YOUNG UNIVERSITY

As chair of the candidate's graduate committee, I have read the thesis of Benjamin M. Faber in its final form and have found that (1) its format, citations, and bibliographical style are consistent and acceptable and fulfill university and department style requirements; (2) its illustrative materials including figures, tables, and charts are in place; and (3) the final manuscript is satisfactory to the graduate committee and is ready for submission to the university library.

_____
Date

_____
Scott D. Sommerfeldt
Chair, Graduate Committee

Accepted for the Department

_____
Ross L. Spencer
Graduate Coordinator

Accepted for the College

_____
G. Rex Bryce, Associate Dean
College of Physical and Mathematical

ABSTRACT

ACTIVE MINIMIZATION OF ACOUSTIC ENERGY DENSITY

IN A MOCK TRACTOR CAB

Benjamin M. Faber

Department of Physics and Astronomy

Master of Science

An active noise control (ANC) system has been applied to the problem of attenuating low-frequency tonal noise inside small enclosures. The intended target application of the system was the reduction of the engine firing frequency inside heavy equipment cabins. The ANC system was based on a version of the filtered-x LMS adaptive algorithm, modified for the minimization of acoustic energy density (ED), rather than the more traditional minimization of squared acoustic pressure (SP). Three loudspeakers produced control signals within a mock cabin composed of a steel frame with plywood sides and a Plexiglas® front. An energy density sensor, capable of measuring acoustic pressure as well as acoustic particle velocity, provided the error signal to the control system. The ANC system operated on a single reference signal, which, for experiments involving recorded tractor engine noise, was derived from the engine's tachometer signal. For the low frequencies at which engine firing occurs,

experiments showed that ANC systems minimizing ED and SP both provided significant attenuation of the tonal noise near the operator's head and globally throughout the small cabin. The tendency was for ED control to provide a more spatially uniform amount of reduction than SP control, especially at the higher frequencies investigated (up to 200 Hz). In dynamic measurement conditions, with a reference signal swept in frequency, the ED control often provided superior results, struggling less at frequencies for which the error sensor was near nodal regions for acoustic pressure. A single control channel often yielded performance comparable to that of two control channels, and sometimes produced superior results in dynamic tests. Tonal attenuation achieved by the ANC system was generally in excess of 20 dB and reduction in equivalent sound level for dynamic tonal noise often exceeded 4 dB at the error sensor. It was shown that temperature changes likely to be encountered in practice have little effect on the initial delay through the secondary control path, and are therefore unlikely to significantly impact ANC system stability in the event that a fixed set of system identification filter coefficients are employed.

ACKNOWLEDGMENTS

I sincerely appreciate the assistance and support of the following people in my efforts to complete this thesis:

- Scott Sommerfeldt, my advisor, for sharing his active noise control expertise with me, and proofreading my thesis;
- Timothy Leishman, for serving on my graduate committee and encouraging me to excel;
- Jonathan Blotter, for serving on my graduate committee and allowing me to share some of the exciting aspects of active noise control with his students;
- Heather Smith, Kent Gee, and Heber Redd, for braving the solder fumes to help construct and repair circuit boards for the control system;
- Lance Locey and Richard Watkins, for their efforts in constructing suitable enclosures for control system electronics;
- Micah Shepherd, Lance Locey, Brian Monson, and Andrew Boone, for assisting with the numerous measurements performed with the control system;
- The BYU Acoustics Research Group, for their support and interest;
- Diann Sorensen and Nan Ellen Ah You, for their essential guidance and support in obtaining materials and filling out the right paper work at the right time;
- Virginia, Benjamin, and Joseph Faber, for the tremendous amount of love and support they have given me all along the way.

TABLE OF CONTENTS

LIST OF FIGURES

Chapter 2

Chapter 3

Chapter 4

Chapter 5

Chapter 6

CHAPTER 1

INTRODUCTION

1.1 Active Noise Control

Although the first patents regarding an electronic system for attenuating sound were filed in the 1930's, active noise control (ANC) research has largely been pursued within the last three decades. In 1936, German physicist P. Lueg was granted a U.S. patent for his proposed electronic system to cancel sound through destructive interference.[1] Lueg's failure to demonstrate a successful noise cancellation system resulted in a general lack of interest in active noise control technology for nearly two decades.

Olson's electronic sound absorber, developed in the early 1950's, provided a feedback mechanism for attenuating low frequency noise near a microphone, but fell short of commercial viability due, in part, to its lack of stability at higher frequencies.[2] The bulk of ANC research has occurred within the last two decades, largely because of recent advances in digital signal processor (DSP) technology as well as the continued development of control theory and adaptive signal processing techniques. Today, ANC systems are found in such places as headphones, high-end automobiles, aircraft, and HVAC systems.

1.2 Interior Cabin Noise

Another potential application for ANC systems is in the attenuation of noise to which heavy equipment operators are exposed. The health and safety of machinery operators can be compromised by the noisy environment in which they spend the bulk of

their time.[3,4] Reducing operator noise exposure has the potential to reduce auditory fatigue and discomfort and increase mental concentration and job efficiency. An additional motivation for noise reduction in tractor cabins is the need of equipment manufacturers to meet current and future international standards for operator exposure to machine noise.

Prior ANC research in tractor cabins showed that the noise spectrum is dominated by discrete tones, which are harmonically related to the tractor engine rotation speed.[3-6] The relatively low frequencies of the engine tones make them especially good candidates for ANC. Passive noise control techniques are quite effective at attenuating high frequencies, but the become impractical in the control of low frequencies.

Although prior efforts to apply ANC to tractor cabins were successful at achieving significant attenuation of the engine tones, significant weaknesses of those systems made them impractical for commercial installation. The spatial region of noise reduction tended to be limited to a fairly small region around the operator's head and error sensors were sometimes placed in impractical locations. An additional drawback in prior active tractor noise control efforts was the inability of control systems to adequately track the rapid changes in engine speed during normal operator work cycles. [3-5]

1.3 Energy Density

In the early 1990's, Sommerfeldt and others at Penn State University showed that minimizing acoustic energy density (ED) can have certain advantages over minimizing squared acoustic pressure (SP) in active noise control applications.[7-10] Active noise control consists of the intentional and careful introduction of acoustic pressure waves

which destructively interfere with existing acoustic pressure waves to reduce the amount of undesired sound in a region of space. In order for an active noise controller to determine an appropriate acoustic pressure to introduce into the system, it must have some criteria for determining what is best, or optimal. Traditionally, active noise control systems use some sort of digital signal processor to implement adaptive algorithms, which provide an optimal solution to the minimization of some error signal. The research performed by Sommerfeldt at Penn State involved the use of acoustic ED as the error signal input to the active control system.[8]

Acoustic ED depends on acoustic particle velocity as well as acoustic pressure. Due to the vector nature of particle velocity, a three-dimensional (3D) ED sensor was developed, which used a two-microphone technique to measure particle velocity in each of three orthogonal directions. The vector sum of the three velocity components from the microphone pairs yields particle velocity and an average of the six microphone signals is used to compute the acoustic pressure. From these quantities, then, the acoustic ED is easily computed.[9]

The research involving the minimization of acoustic ED investigated noise reduction in enclosed sound fields. One of the main advantages enjoyed by energy-based control is its reduced sensitivity to error sensor placement within these fields. In a rectangular enclosed sound field, there are nodal planes for the acoustic pressure, which exist in the three orthogonal directions. However, for ED there are only nodal lines, which exist at the intersection of two orthogonal nodal planes of the pressure. Therefore, for a given error sensor location, an ED sensor has a much higher probability of being placed in a region away from nodes, where it can adequately observe an acoustic mode.[10]

If an error sensor were located in a nodal region for a particular mode, the control system would not be able to reduce the energy in that mode, because it would not even detect the mode in the first place.

Another advantage of energy density is its ability to provide more global attenuation of the noise. In other words, the spatial region in which the undesired noise is attenuated tends to be larger for ED than for SP. This may be because an ED sensor gathers more information about the acoustic field than a simple pressure sensor. While the ED control system is able to provide attenuation of broadband noise signals, the most dramatic effects have been seen when attacking tonal noise, especially when that tonal noise coincides, in frequency, with a natural frequency of the enclosure.[7]

The original ED-based ANC system, developed at Penn State, now resides at Brigham Young University.

1.4 Research Overview

Due to the need for an active noise control system which can provide significant noise reduction over a large spatial region within a tractor cab, and to do so unobtrusively in all machine conditions (static and dynamic), the active minimization of ED has been applied to reduction of tractor engine noise within the tractor cab. The main objectives of this research project have been to verify the successful operation of an ED-based control system in a mock tractor cab and to document its performance in terms of global noise attenuation under static and dynamic engine speed conditions.

1.5 Thesis Organization

Chapter 2 discusses acoustic energy density in greater detail as well as a method for measuring it. Chapter 3 then discusses the acoustics encountered in typical tractor cabs, including the effects of the acoustics on noise control efforts as well as the characteristics of the noise commonly present in such cabs. The ANC algorithm used in this research is presented in Chapter 4, after which an explanation of the experimental setup appears in Chapter 5. Chapter 6 includes the presentation and discussion of measurement results. Conclusions and recommendations for future research constitute Chapter 7.

CHAPTER 2

ACOUSTIC ENERGY DENSITY

The total energy in an acoustic field is composed of both potential and kinetic energy quantities. The potential energy is a function of acoustic pressure, and the kinetic energy is a function of the acoustic particle velocity. The potential acoustic energy can be expressed as

$$E_p = \frac{1}{2}\left(\frac{p^2}{\rho_0 c^2}\right)V_0, \tag{2.1}$$

where p, ρ_0, c, and V_0 represent acoustic pressure, the ambient fluid density, the speed of sound, and an infinitesimal volume containing the total potential energy, E_p. In this thesis the fluid of interest is air. The total kinetic energy of an infinitesimal volume of air is given by

$$E_k = \frac{1}{2}\rho_0 V_0 \vec{u}\cdot\vec{u} = \frac{1}{2}\rho_0 V_0 u^2, \tag{2.2}$$

where $\vec{u}$ is the acoustic particle velocity vector. Summing the two energy quantities and dividing by V_0 yields the total instantaneous acoustic ED:

$$e_i = \frac{1}{2}\rho_0\left[u^2 + \left(\frac{p}{\rho_0 c}\right)^2\right]. \tag{2.3}$$

2.1 Measuring Energy Density

In order to use acoustic ED as an error signal for a control system utilizing an adaptive filter, ED must be measured in real time. By assuming the density of air and the speed of sound in air to be constant (and known), only acoustic pressure and particle velocity need to be measured in order to obtain a measurement of ED. A two-

microphone technique allows a single directional component of particle velocity to be measured along the line passing through both microphones.

Euler's equation relates the acoustic particle velocity to pressure as follows:

$$\rho_0 \frac{\partial}{\partial t} \vec{u} = -\nabla p. \tag{2.4}$$

Solving for a single component of particle velocity, $\vec{u}$, in the x direction, yields

$$u_x = -\frac{1}{\rho_0} \int \frac{\partial}{\partial x} p dt. \tag{2.5}$$

The spatial derivative of the pressure can be approximated in the x direction (and similarly in the y and z directions) by a difference of two pressures measured a small distance Δx apart:

$$u_x \approx -\frac{1}{\rho_0} \int \frac{p_2 - p_1}{\Delta x} dt. \tag{2.6}$$

Equation 2.6 yields a continuous time expression for the x component of particle velocity. However, since the calculation is to be performed within a DSP, the integral takes the form of a sum for discrete time implementation of the measurement:

$$u_x \approx -\frac{\Delta t}{\rho_0 \Delta x} \sum (p_2 - p_1). \tag{2.7}$$

All three components of the particle velocity at a single point can be found in this manner, using three orthogonally arranged pairs of microphones. The pressure value used in the ED measurement is found by taking the average of the pressures measured by the six microphones.

Parkins, *et al.*[9] described the errors associated with the aforementioned energy density sensor developed in conjunction with early research of energy-based ANC systems. As shown in Figure 2.1, the 3D ED sensor consists of six inexpensive electret

microphones embedded in a 2-inch diameter wooden sphere. The inside of the wooden sphere is hollowed out in order to house electronics for microphone signal amplification. A 9-pin D-Sub connector is used to connect the sensor to the ANC system electronics.

Figure 2.1 3D ED sensors. The left sensor is open to reveal the electronics.

If the microphones are poorly matched, sensitivity and phase mismatch of the microphones will dominate the bias error of the ED sensor. The microphones employed in the 3D sensors were matched to within ±0.25 dB of sensitivity and ±1 degree of phase at 100 Hz. The errors in the measurement of the kinetic and potential energies are then largely due to the sum and difference approximations used to measure the particle velocity and pressure. However, errors in the energy density due to these approximations turn out to be relatively small. The reason for this is that the errors are greatest in the estimation of kinetic or potential energy when that quantity is small. However, for an enclosed sound field, when the kinetic energy is small the potential energy is typically large, and vice versa. This means that the quantity suffering least from bias errors contributes most to the estimation of total energy density. This effect vanishes at

extremely low frequencies. It was shown that the (2-inch) 3D ED sensor could be built to keep the total energy density errors within ±1.75 dB in the frequency range $110 < f < 400$ Hz.[9]

The presence of the wooden sphere itself contributes to the bias errors of the sensor, but this contribution turns out to be beneficial.[11] The two-microphone technique for measuring particle velocity assumes that some distance d separates the two microphones, with no obstruction between them. The insertion of a sphere between two microphones requires a sound wave to travel further from one to the other than if there were no sphere present. The net result is that a spherical particle velocity sensor behaves similar to a pair of microphones with no (or negligible) obstruction between them and separated by 1.5 times the diameter of the sphere. The use of a sphere thus allows the ED sensor to be built two-thirds the size of an ED sensor with no sphere, without a loss in accuracy. Energy density sensors employing microphone arrangements different than that described above have also been explored at Brigham Young University.[12]

CHAPTER 3

CAB ACOUSTICS

Modern equipment cabs often provide some passive noise attenuation for the operator, as well as some additional comforts, by completely enclosing the sound field in which the operator sits. For some initial acoustical analysis, a rigid-walled, rectangular box can generally approximate the shape of these cabs quite well. Therefore, understanding the acoustical environment inside of a cab begins with an understanding of rectangular, enclosed sound fields.

3.1 Rectangular Enclosed Sound Fields

In a rectangular enclosure with rigid boundaries, the component of acoustic particle velocity normal to each boundary must vanish. Euler's equation then yields the following boundary conditions for the acoustic pressure:

$$\left.\begin{aligned}\nabla_x p = 0\\ \nabla_y p = 0\\ \nabla_z p = 0\end{aligned}\right\} \text{ for } \begin{cases} x = 0, L_x \\ y = 0, L_y \\ z = 0, L_z \end{cases}, \tag{3.1}$$

where L_x, L_y, and L_z are the dimensions of the enclosure in the x, y, and z directions, respectively. The acoustic pressure can be assumed to have a time dependence of $e^{j\omega t}$, and treated as a function of position only, which will satisfy the homogeneous Helmholtz equation,

$$\nabla^2 p + k^2 p = 0, \tag{3.2}$$

where k is the acoustic wavenumber, given by $k = \omega/c$. The separation of variables technique can be used to find a solution by substituting the following expression for pressure into the Helmholtz equation:

(3.3)

$$p(x,y,z) = X(x)Y(y)Z(z).$$

This yields three separate equations in x, y, and z, which have solutions that can be written in terms of sine and cosine functions to reflect the standing wave behavior of an enclosed sound field. Application of the boundary conditions reduces the final solution for each equation to a cosine term.

A general solution to the Helmholtz equation can be written as a sum of its eigenfunctions, which in this case correspond to the acoustic modes of the enclosure.

$$p(x,y,z) = \sum_{l=0}^{\infty}\sum_{m=0}^{\infty}\sum_{n=0}^{\infty} A_{lmn}\cos k_x x \cos k_y y \cos k_z z, \tag{3.4}$$

where A_{lmn} is an arbitrary complex constant, ${k_{lmn}}^2 = {k_x}^2 + {k_y}^2 + {k_z}^2$, and

$$k_x = \frac{l\pi}{L_x},\ k_y = \frac{m\pi}{L_y}, \text{ and } k_z = \frac{n\pi}{L_z}. \tag{3.5}$$

This means that any acoustic field within a rigid-walled, rectangular enclosure can be described by a weighted sum of the acoustic modes of the enclosure. Since it has been shown that sound fields in lightly damped enclosures can be accurately described using the rigid-walled eigenfunctions, the following discussion of enclosed sound fields assumes that tractor cabin interiors exhibit low damping.[13]

3.2 Active Control in Enclosed Sound Fields

The presence of nodal regions associated with modes in an enclosed sound field can result in observability problems for an ANC system. If an error sensor of the system is located at, or near, a node for a particular mode, the sensor will not be able to observe that mode. In this case, the control system will be unable to control undesired noise at the frequency corresponding to the given mode. Another problem arises when the system

allows the energy in that mode to be amplified in its efforts to control noise present in other modes. This is called spillover.

The two approaches to active control already mentioned rely on error sensors that measure SP or ED, respectively. The spatial dependence for the normalized SP of the (l,m,n) mode is

$$p_{lmn}^2 = \cos^2 k_x x \cdot \cos^2 k_y y \cdot \cos^2 k_z z \tag{3.6}$$

and is shown in two dimensions in Figure 3.1 for the (1,1,0) mode.

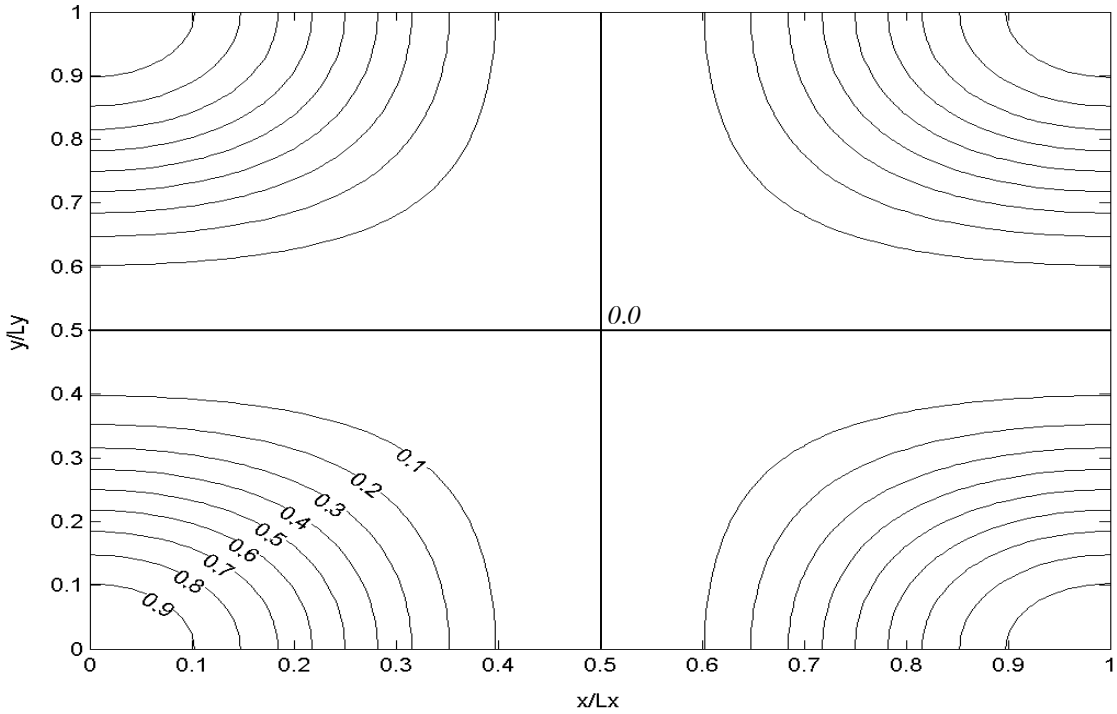

Figure 3.1 Spatial dependence of (normalized) squared pressure for the (1,1,0) mode (after Parkins[10]).

From this, it is easy to see that a nodal plane will exist in a three-dimensional enclosure whenever any one of the cosine terms goes to zero. The spatial dependence for normalized ED is given by

$$e_{lmn} = \frac{1}{k^2}(k_x^2 \cos^2 k_y y \cdot \cos^2 k_z z + k_y^2 \cos^2 k_x x \cdot \cos^2 k_z z + k_z^2 \cos^2 k_x x \cdot \cos^2 k_y y) \tag{3.7}$$

and is shown in Figure 3.2 for the (1,1,0) mode. Two cosine terms must vanish simultaneously in order to produce a node in the energy density field. This corresponds to the location at which nodal planes in the pressure field intersect. The significance of this is that an error sensor that measures energy density has a much lower probability of being unable to observe a given mode in a particular location within the enclosure.[10]

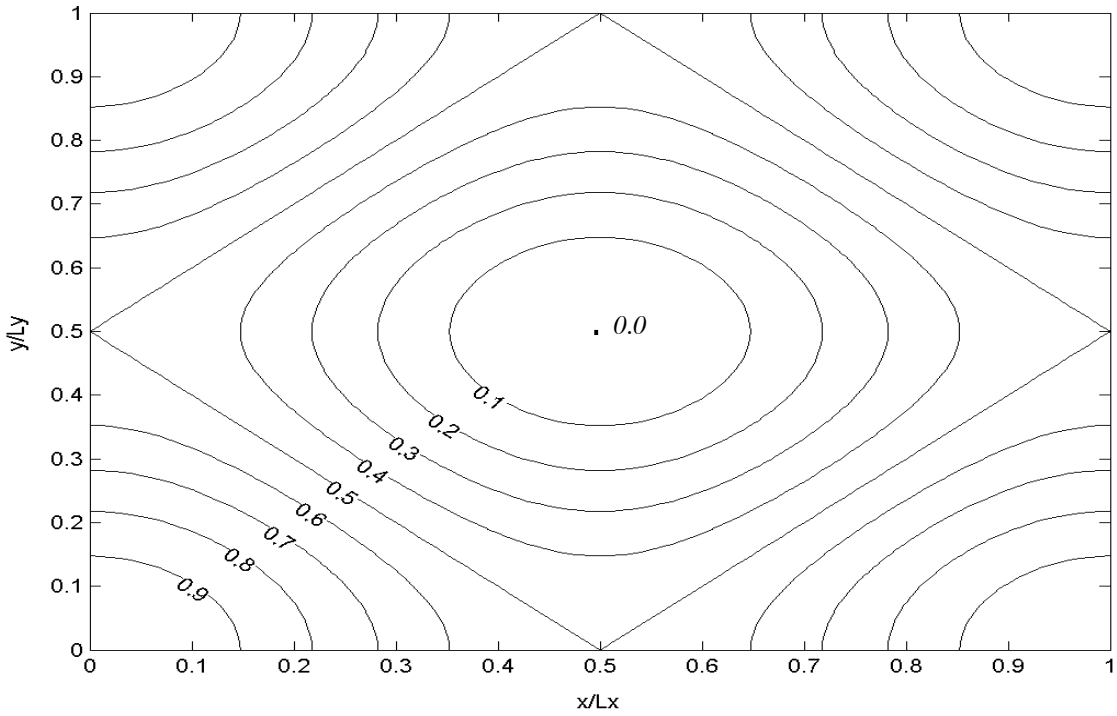

Figure 3.2 Spatial dependence of (normalized) energy density for the (1,1,0) mode (after Parkins[10]).

3.3 Noise in Tractor Cabs

As mentioned in section 1.2, the noise inside a tractor cab is dominated by tonal components that are harmonically related to the rotation speed of the engine. For a typical six-cylinder machine, the engine firing frequency is three times that of the engine rotation frequency and is generally the dominant tonal component of the noise inside the cab. This engine firing frequency can be as low as 40 Hz and extend up to the 100 to 200

Hz range. The research presented in this thesis explored the performance of an ANC system targeting only a single tone inside the mock cabin at any one time. The presence of strong tonal components in the noise suggests that situations might arise when ED-based ANC could have a significant advantage over SP-based ANC, depending on error sensor location and modal shape.

CHAPTER 4

ALGORITHM DEVELOPMENT

The ANC system described in this thesis incorporates a feedforward adaptive filtering algorithm. This algorithm is a version of the Filtered-X algorithm, which is commonly used in ANC applications, but which has been modified for the minimization of acoustic energy density rather than squared acoustic pressure.

4.1 Feedforward Control

Feedforward control systems tend to be preferred over feedback systems when the application lends itself to their use. Feedforward systems depend on some reference signal that allows the incoming noise to be predicted in advance, so that a suitable control signal can be generated in time to counteract the noise. In cases where a suitable reference signal cannot be found, feedback control becomes the only alternative. Feedforward control is most often applied to situations in which the noise to be attenuated is periodic. For applications in which either feedforward or feedback control can be used, feedforward control provides greater noise reduction and stability.

Generally, the means by which feedforward control systems attenuate noise is the principle of superposition of acoustic waves. The principle of superposition can be employed in the alteration of the acoustic radiation impedance seen by the noise source such that the amount of acoustical energy radiated by the source is minimized. Feedforward systems can also cause the control sources to absorb acoustical energy, but this yields suboptimal performance.[14]

4.2 The Control Algorithm

Feedforward ANC systems generally employ adaptive signal processing techniques, together with DSP technology, to filter the reference signal in such a way that the residual noise, measured by some error sensor, will be minimized. Even slight changes in the physical environment in which the control is employed can lead to significantly degraded performance for a fixed set of filter coefficients. For this reason, it makes sense for modern ANC systems to be able to continuously adapt to changes in the physical plant or the reference signal. The ANC system of interest, here, employs the filtered-x LMS algorithm, which is based on the more widely known LMS algorithm.

4.2.1 Steepest Descent

Adaptive signal processing generally involves finding some vector of filter coefficients, $\mathbf{w}_n$, which minimizes a quadratic cost function at time n. The variable, n, is used throughout the following discussion as a discrete time index. The method of steepest descent is an iterative approach to finding the extrema of quadratic functions, which provides a basis for the LMS algorithm. The method of steepest descent uses the gradient of the cost function to provide updates to $\mathbf{w}_n$. The gradient of the cost function is the vector of partial derivatives with respect to each of the elements of $\mathbf{w}_n$, and points in the direction of maximum ascent up the quadratic surface (away from its unique global minimum). With each iteration, $\mathbf{w}_n$ takes a step of size μ times the gradient in the direction opposite that of the gradient. This is often expressed as

$$\mathbf{w}_{n+1} = \mathbf{w}_n - \mu \nabla \xi(n), \tag{4.1}$$

where $\xi(n)$ is the cost function, defined as a mean squared error.

A typical application which can be used to demonstrate the method of steepest

descent, as well is its practical implementation in the form of the LMS algorithm, is that of attenuating the output of an unknown system by filtering its input with a finite impulse response (FIR) filter and adding the result to its output. The FIR filter is determined adaptively, as shown in Figure 4.1.

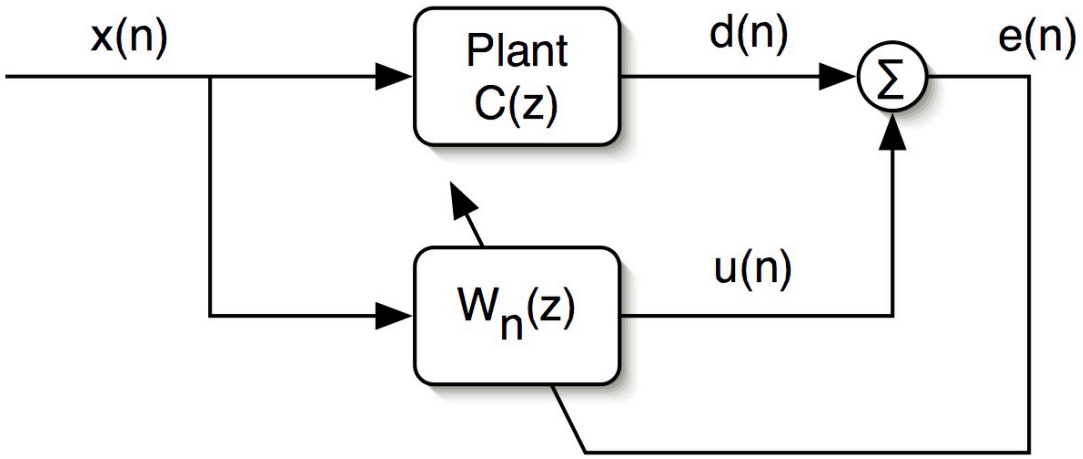

Figure 4.1 Block diagram of the LMS adaptive algorithm.

The signals x(n) and u(n) are treated as random processes, and $\mathbf{w}_n$ is treated as a vector containing the coefficients of the FIR filter, $W_n(z)$, where z represents the discrete frequency variable. The goal is to find $\mathbf{w}_n$ which minimizes the mean-square error (MSE),

$$\xi(n) = E\left[|e(n)|^2\right], \tag{4.2}$$

where

$$e(n) = d(n) + u(n) = d(n) + \sum_{l=0}^{p} w_{l,n} x(n-l) = d(n) + \mathbf{w}_n^T \mathbf{x}(n). \tag{4.3}$$

In this expression, p is the order of the filter represented by **w**, and **x**(n) is the (p+1)x1 vector containing the current and past samples of x(n). If **w** is assumed to be complex, finding the gradient of the cost function means taking the derivative of $E[|e(n)|^2]$ with

respect to w*, where * denotes a complex conjugate:

$$\nabla E\left[|e(n)|^2\right] = E\left[\nabla|e(n)|^2\right] = E\left[e(n)\nabla e^*(n)\right]. \tag{4.4}$$

Since $\nabla e^*(n) = \mathbf{x}^*(n)$, then

$$\nabla\xi(n) = E\left[e(n)\mathbf{x}^*(n)\right], \tag{4.5}$$

and

$$\mathbf{w}_{n+1} = \mathbf{w}_n - \mu E\left[e(n)\mathbf{x}^*(n)\right]. \tag{4.6}$$

When d(n) and x(n) are jointly wide-sense stationary random processes, the adaptive filter employing the method of steepest descent converges to the solution of the Wiener-Hopf equations,

$$\lim_{n\to\infty}\mathbf{w}_n = -\mathbf{R}_x^{-1}\mathbf{r}_{dx}, \tag{4.7}$$

where $\mathbf{R}_x$ is the Hermitian Toeplitz autocorrelation matrix of the input signal,

$$\mathbf{R}_x = E\left[\mathbf{x}(n)\mathbf{x}^H(n)\right], \tag{4.8}$$

and $\mathbf{r}_{dx}$ is the vector of cross-correlations between d(n) and x(n).[15] An additional constraint on convergence is that μ, which controls the step size, must be greater than zero and less than $2/\lambda_{max}$ where λ_{max} is the largest eigenvalue of the autocorrelation matrix $\mathbf{R}_x$. In this case, the solution to the Wiener-Hopf equations represents the global minimum of the quadratic function, or "bottom of the bowl."

4.2.2 The LMS Algorithm

The problem with the practical implementation of the method of steepest descent stems from the fact that the expectation $E[e(n)\mathbf{x}^*(n)]$ is generally unknown. The solution to that problem is to replace the expectation with an estimate

$$\hat{\nabla}\xi(n) = \hat{E}\left[e(n)\mathbf{x}^*(n)\right] = \frac{1}{L}\sum_{l=0}^{L-1} e(n-l)\mathbf{x}^*(n-l), \tag{4.9}$$

which can become computationally expensive, especially with the real-time constraints encountered in active noise control applications. The LMS algorithm uses a single-point estimate of the expectation,

$$\hat{E}\left[e(n)\mathbf{x}^*(n)\right] = e(n)\mathbf{x}^*(n), \tag{4.10}$$

so the LMS adaptive filter update equation becomes

$$\mathbf{w}_{n+1} = \mathbf{w}_n - \mu e(n)\mathbf{x}^*(n), \tag{4.11}$$

which is less expensive from a computational standpoint. Although this is a crude estimate of the gradient of the cost function, it is known to work successfully in practice. The update to the vector **w** will not generally be in the direction of steepest descent, but the single-point estimate of the gradient is unbiased:

$$\hat{\nabla}\xi(n) = E\left[e(n)\mathbf{x}^*(n)\right] = \nabla\xi(n). \tag{4.12}$$

This means that, on average, the updates to **w** will be in the direction of steepest descent. The LMS adaptive algorithm converges in the mean as long as the same constraint on μ is met as for the method of steepest descent. However, to determine an appropriate value for μ to yield stable convergence would require an estimate of λ_{max}. An upper bound for λ_{max} is the trace of the input autocorrelation matrix, tr($\mathbf{R}_x$), which can itself be expressed as $(p+1)E[|x(n)|^2]$ for a wide sense stationary input signal. Again, this expected value will generally be unknown, but can be estimated with a sample average, which is easier than estimating the eigenvalues of $\mathbf{R}_x$. The bounds on μ for the LMS algorithm then become:

$$0 < \mu < \frac{2}{(p+1)\hat{E}\left[|x(n)|^2\right]} \tag{4.13}$$

where

$$\hat{E}\left[|x(n)|^2\right] = \frac{1}{N}\sum_{k=0}^{N-1}|x(n-k)|^2 \qquad (4.14)$$

Widrow and Stearns[16] suggest that a typical step size to use is one tenth of the upper bound given in Equation 4.13.

4.2.3 Filtered-x Algorithm

The trouble with the system described in Figure 4.1 is that active noise control systems are trying to measure and attenuate some acoustical error signal. This means that the control signals must add acoustically with the undesired noise. A more realistic diagram of this scenario is shown in Figure 4.2, which includes the path through which a control signal must travel after it leaves the DSP and before it returns to the DSP as a contribution to the error signal. This secondary path, as it is sometimes called, includes effects from the digital-to-analog converter (DAC), reconstruction filter, audio power amplifier, loudspeaker(s), acoustical transmission path, error sensor(s), signal conditioning electronics, antialias filters, and analog-to-digital converter (ADC). In general, this secondary path will cause instability when introduced into a controller which employs the standard LMS algorithm.[17] Morgan proposed two possible solutions to this problem and a short time later, one of those solutions, independently developed by Widrow and Burgess, became known as the filtered-x LMS algorithm (sometimes written FXLMS).[13, 17] The following discussion assumes all signals to be real, not complex.

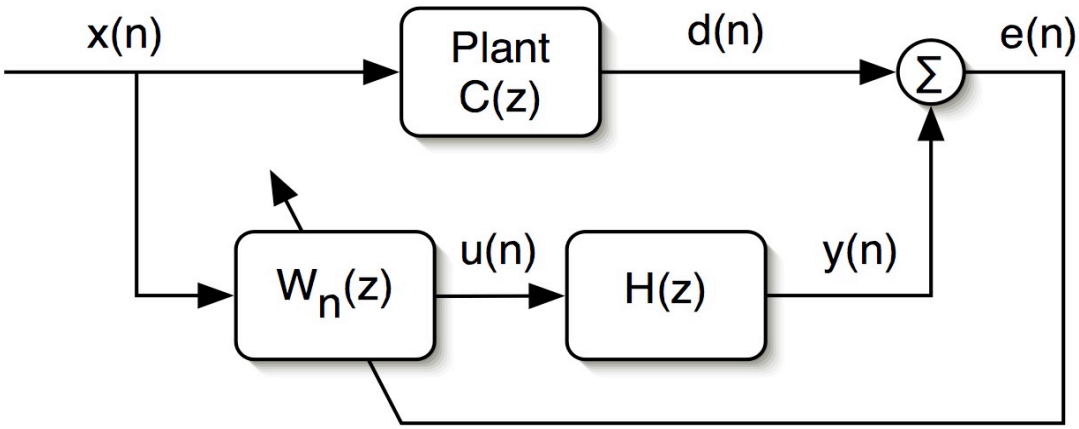

Figure 4.2 Block diagram of the filtered-x LMS algorithm for acoustic systems.

The incorporation of the secondary path transfer function into the existing LMS algorithm is fairly straightforward. For a linear, time-invariant (LTI) system, the order of the control filter, W, and the secondary path, H, may be reversed. Mathematically, in the frequency domain

$$\begin{aligned} E(z) &= D(z) + H(z)U(z) = D(z) + H(z)W(z)X(z) \\ &= D(z) + W(z)H(z)X(z) = D(z) + W(z)R(z), \end{aligned} \tag{4.15}$$

so the time domain error signal can be written

$$e(n) = d(n) + \mathbf{w}^T \mathbf{r}(n). \tag{4.16}$$

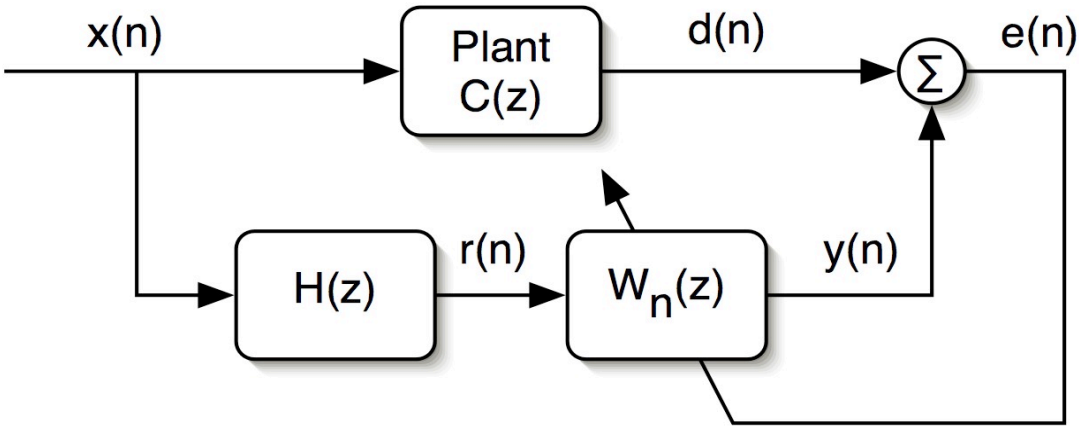

Figure 4.3 Block diagram of the filtered-x LMS algorithm with the secondary path transfer function, H(z), and the control filter, $W_n(z)$, interchanged.

Since a single point estimate of the expectation is used, the quadratic cost function becomes simply the instantaneous squared error.

$$\xi(n) = e^2(n) = d^2(n) + 2d(n)\mathbf{w}^T\mathbf{r}(n) + \mathbf{w}^T\mathbf{r}(n)\mathbf{r}^T(n)\mathbf{w}. \tag{4.17}$$

The gradient of the squared error now becomes

$$\frac{\partial e^2(n)}{\partial \mathbf{w}} = 2d(n)\mathbf{r}(n) + 2\mathbf{r}(n)\mathbf{r}^T(n)\mathbf{w} = 2e(n)\mathbf{r}(n) \tag{4.18}$$

and the control filter update equation can be written as

$$\mathbf{w}_{n+1} = \mathbf{w}_n - \mu e(n)\mathbf{r}(n). \tag{4.19}$$

A challenge associated with the inclusion of secondary path effects in the control algorithm, is that the secondary path, represented by H(z) in Figure 4.3, is unknown. An estimate of the secondary path is obtained through the process of system identification, discussed in the next section, and is used to produce the so-called filtered-x signal, r(n). After the control filter coefficients are updated according to Equation 4.19, they are used to filter the reference signal, x(n), directly in order to produce the desired control signal at the location of the error sensor. Figure 4.4 illustrates this in a block diagram.

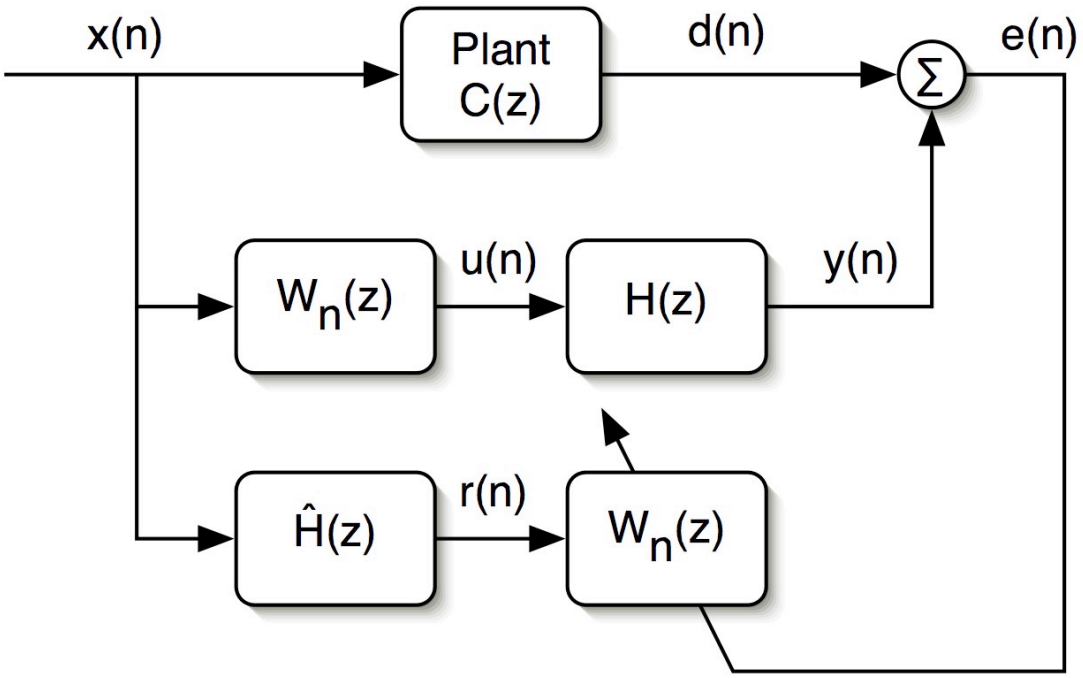

Figure 4.4 Block diagram of the filtered-x LMS algorithm.

4.2.4 Modified Filtered-x Algorithm

The filtered-x LMS algorithm described above is often used in ANC systems which employ pressure sensors to obtain a squared acoustic pressure as an error signal. As already discussed, acoustic energy density depends on acoustic pressure as well as acoustic particle velocity, which itself is composed of three directional components. For this reason, the standard filtered-x algorithm must be modified in order to minimize acoustic energy density. A block diagram of the filtered-x algorithm, modified for energy density, is shown in Figure 4.5.

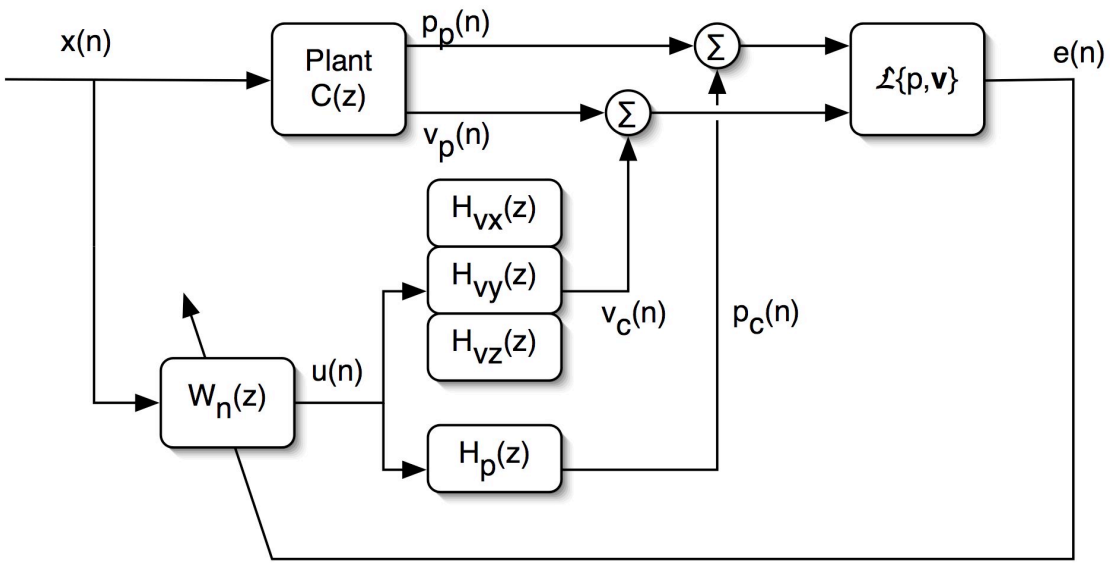

Figure 4.5 The filtered-x algorithm, modified for minimization of energy density.

As can be seen in the block diagram, secondary paths must be considered for each of the three components of the particle velocity as well as the pressure path. Models must be obtained for each of these paths in order for the control filter coefficients to be updated properly. Alternatively, these paths can be thought of as components of a single secondary path. The so-called filtered-x signal, r(n), then becomes, in reality, four filtered-x signals, $r_p(n)$, $r_{vx}(n)$, $r_{vy}(n)$, and $r_{vz}(n)$, each produced by filtering the reference signal with the appropriate component of the secondary path. The block labeled £{p,**v**} is included to designate the processing which takes place in order to compute an actual energy density quantity from the pressure and velocity components. The update equation for the modified algorithm is

$$\mathbf{w}_{n+1} = \mathbf{w}_n - \mu\left(\frac{p(n)}{\rho_0 c^2}\mathbf{r}_p(n) - \sum_{m=1}^{3}\frac{u_m(n)}{\Delta x}\mathbf{r}_{vm}(n)\right), \tag{4.20}$$

where $u_m(n)$ is the m^{th} component of the instantaneous particle velocity at time n.[8]

4.3 System Identification

As mentioned in the previous section, the filtered-x algorithm, which has been modified for energy density, assumes that the secondary control path is known for all components of the acoustic particle velocity as well as for acoustic pressure. The process of measuring this response is referred to as system identification (SysID). The model of the secondary path, obtained through system identification, is a discrete time impulse response that filters the reference signal to produce the filtered-x signals.

4.3.1 Offline Versus Online System Identification

System identification can be performed online, while the ANC system itself is running, or offline, before the control system is started. Each approach carries certain implications on the performance of the ANC system. Offline system identification, by itself, assumes that the secondary path is time-invariant. Significant changes in the secondary path can have adverse effects on the stability of the ANC system when a fixed model of that path is used. Online system identification, which generally incorporates a second adaptive filter, has the advantage of being able to adapt to changes in the secondary path, but can slow the convergence of the ANC system in the process. An alternative to using either approach by itself would be to use some combination of the two. In that case, an a priori estimate of the secondary path would provide for rapid convergence of the ANC algorithm at the start, but adaptive (online) system identification would provide greater long-term stability to the system. The research discussed in this thesis used offline system identification exclusively, in an effort to provide the fastest possible convergence of the ANC system. Some of the effects of changes to the secondary path on stability of the ANC system have been explored for the case of a fixed

secondary path model.

4.3.2 The System Identification Algorithm

As in the case of the filtered-x algorithm, the offline system identification performed for this research produces an FIR filter. Although system identification is often performed with adaptive filters, which yields a Wiener filter with stationary input signals, the present system solves for the Wiener filter directly. A block diagram of the system is shown in Figure 4.6.

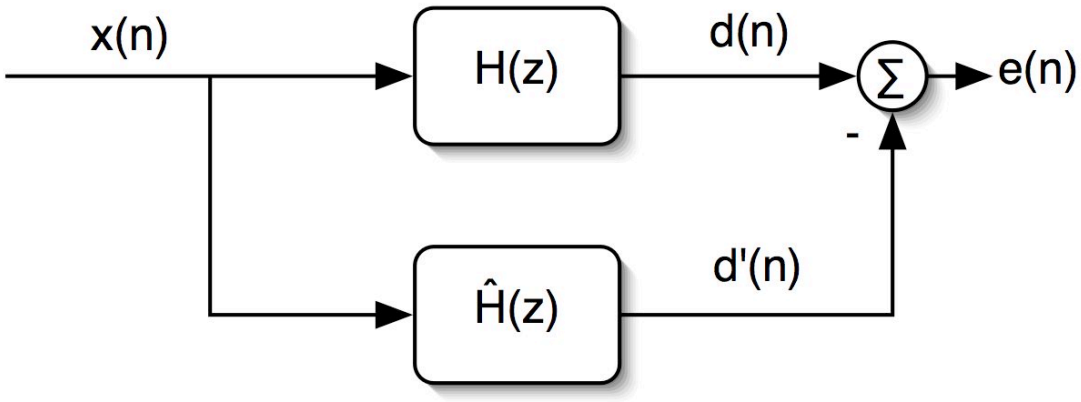

Figure 4.6 Offline system identification using an FIR Wiener filter.

As shown in the figure above, a model of the unknown secondary path, H, is to be found. Since the ANC system is not running, a known signal can be injected into the unknown system, and the output measured. White noise is chosen as the input signal, because white noise is stationary and its autocorrelation function is merely a delta function. The FIR Wiener filter is given by the solution to the Wiener-Hopf equations as

$$\hat{\mathbf{h}} = \mathbf{R}_x^{-1}\mathbf{r}_{dx}, \tag{4.21}$$

where $\mathbf{R}_x$ is the auto correlation matrix of the input signal, x(n), and $\mathbf{r}_{dx}$ is the cross-correlation vector of the output signal, d(n), and the input signal. This solution minimizes the mean squared error (MSE), e(n), which is defined as the difference

between the output of the true path, d(n), and the output of the model, d'(n). Because x(n) was chosen to be white noise, with a delta function describing its autocorrelation, its autocorrelation matrix is simply a diagonal matrix, which is easily invertible. The equation that yields the appropriate secondary path model then becomes

$$\hat{\mathbf{h}} = \mathbf{R}_{\mathbf{x}}^{-1}\mathbf{r}_{\mathbf{dx}} = \frac{1}{r_x(0)}\mathbf{r}_{\mathbf{dx}}. \tag{4.22}$$

The minimum mean squared error (MMSE) is then given by

$$\xi_{\min} = r_d(0) - \mathbf{r}_{\mathbf{dx}}^{\mathrm{T}}\hat{\mathbf{h}} = r_d(0) - \frac{1}{r_x(0)}\mathbf{r}_{\mathbf{dx}}^{\mathrm{T}}\mathbf{r}_{\mathbf{dx}}. \tag{4.23}$$

4.3.3 System Identification and ANC System Stability

The quality of the secondary path model, obtained via system identification, impacts the stability and convergence speed of the ANC algorithm. Widrow and Stearns[16] suggest that the secondary path model must have at least as much delay in its impulse response as the true path. Kuo and Morgan[17] showed that in order to maintain stability of the filtered-x algorithm, the phase response of the secondary path model must be within 90º of the true secondary path. However, as the phase difference approaches 90º, the convergence of the algorithm slows.

CHAPTER 5

EXPERIMENTAL SETUP

5.1 The Cab

The enclosure in which the control system was operated, and its performance measured, resembles a typical enclosed tractor cabin. The mock cab measures 1.5 meters in height and 1 meter in width. From front to back, the cab is 1 meter long at the top and 1.2 meters long at the bottom. The floor, ceiling, side, and back walls of the cab are constructed of 3/8-inch plywood, while the front is constructed of 1/8 inch Plexiglas®. The frame is of rigid steel. A chair was placed at the back of the mock cab, in order for a person to sit inside, as a machinery operator would in a real cab, and operate the control system. Photos of the cab appear in Figure 5.1.

Figure 5.1 Mock cabin photos. Front and side views on the left and right, respectively.

A full-range loudspeaker with reasonably flat frequency response down to 37 Hz was placed underneath the operator's seat, as shown in Figure 5.1. This loudspeaker was used to inject various types of noise into the cab, in order to test the performance of the ANC system. The loudspeaker was placed inside the cab for convenience, as well as to minimize the annoyance of the tests to persons in and around the lab who were not involved in the research. Placing the loudspeaker outside of the cab should more closely resemble an actual tractor, which produces noise with the engine outside its own cab. However, much of what this research intended to discover should not have been affected much by locating the noise source inside the mock cabin.

Modal analysis of the mock cab was performed with the Finite Element Method using LMS SYSNOISE to provide color maps of mode shapes up to 200 Hz. The boundaries were assumed to be rigid. Figures 5.2 through 5.5 contain the resulting color maps for the first four modes. The dark blue color indicates a nodal region.

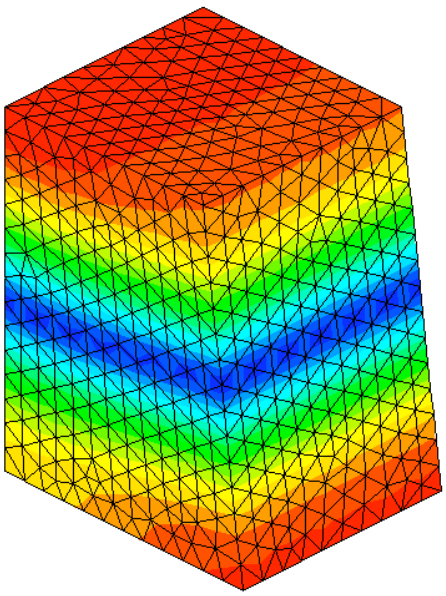

Figure 5.2 (0,0,1) mode at 113.2 Hz.

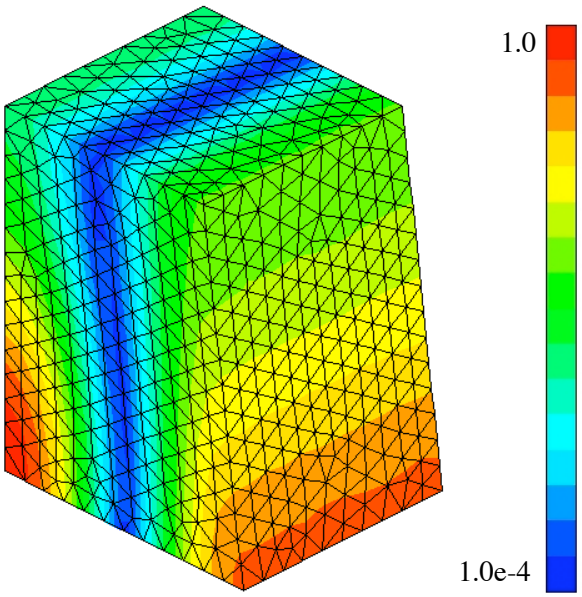

Figure 5.3 (0,1,0) mode at 154.0 Hz.

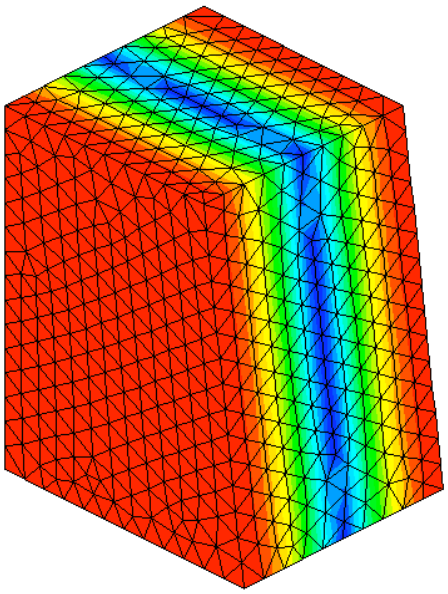

Figure 5.4 (1,0,0) mode at 170.8 Hz.

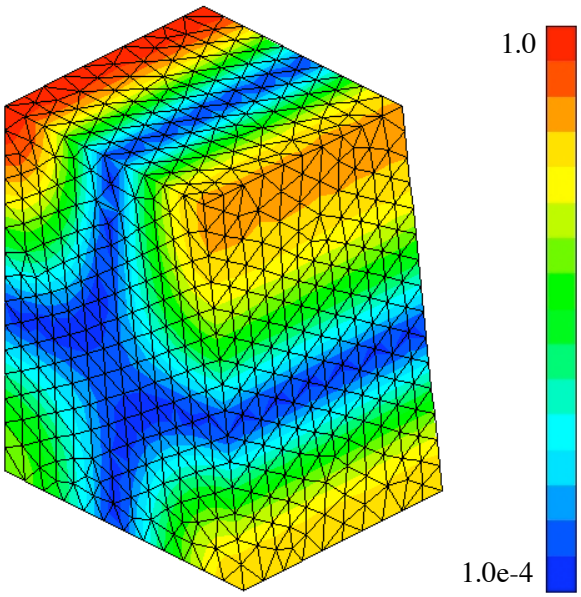

Figure 5.5 (0,1,1) mode at 194.8 Hz.

5.2 Sensors and Actuators

5.2.1 Energy Density Sensors

A single ED sensor was placed near the ceiling of the mock cabin so as to be situated directly above the operator's head. The use of a single error sensor yields reduced component and computational costs as opposed to a multiple sensor ANC system. Additionally, since the area of maximum attenuation tends to be centered on the error sensor, it seemed appropriate to center the sensor above the region where the operator's head would be most of the time. This region is generally centered between the two side walls of the cab and is usually close to the back wall. The use of two sensors, one on either side of the operator's head, would present the possibility of the zone of silence being shifted to one side or the other, which would be undesirable. Placing a single sensor close to the ceiling above the operator's head also made it unobtrusive. In this configuration, the third mode of the cab (Figure 5.4) would present a problem for a

SP sensor because of the nodal region centered between the two side walls of the cab. The error sensor could also be close to the nodal regions of the second and forth modes, shown in Figures 5.3 and 5.5, respectively. The proximity of the sensor to the operator's head suggests that the operator may not easily observe the noise in those modes either. However, ED control would be expected to provide better attenuation of the noise throughout the cab at those modal frequencies, which would be most meaningful if the operator were to lean forward or to one side of the normal upright sitting position.

5.2.2 Control Actuators

A total of three loudspeakers were used as control actuators for the ANC system. Two smaller satellite speakers were place on either side of the operator's head at essentially the same height as the operator's ears. In this location, the loudspeakers do not lie within a nodal region for any of the first four modes of the cab. This ensures that each of those modes can be sufficiently excited by the loudspeakers. Generally, the ANC system employed two control channels, one for each of the two satellite speakers. Because of the size of the satellite speakers, they are not adequate to control low frequency noise inside the cab. For this purpose, a subwoofer was placed on the floor of the cab in a corner, also away from nodal regions. The control signals produced by the ANC system were high pass filtered with a 90 Hz cutoff frequency before being sent to each of the satellite speakers. The control signals were summed and low pass filtered with the same (90 Hz) cutoff frequency before being passed to the subwoofer. Some single control channel experiments were conducted as well and are discussed in Chapter 6.

A photo showing the locations of the two satellite speakers as well as the ED error

sensor is shown in Figure 5.6. The location of the subwoofer can be seen in Figure 5.1.

Figure 5.6 Satellite control speakers and ED error sensor placement.

5.3 Control System Electronics

A custom control system was developed for the purposes of this research. It incorporates a Texas Instruments (TI) TMS320VC33 DSP processor, with a custom input/output (I/O) board, an error sensor, signal conditioning electronics for the error sensor, reference, and control signals, and new control speakers. The algorithm was translated from assembly code, originally developed at Penn State for a Motorola 96002 DSP processor, into C code to be run on the new DSP. C code will also allow for easier portability in the future. The electronics were designed to maintain compatibility with the original 3D ED sensors. They also operate on a standard 12-Volt power supply that offers the potential for experiments on actual tractors.

5.3.1 Digital Signal Processor

The TMS320VC33 DSP operates on a 60 MHz clock and has the capacity for 60 million instructions per second (MIPS) or 120 million floating-point operations per second (MFLOPS). The accompanying I/O board supplies 8 input and 4 output channels, via 12-bit analog-to-digital converters (ADC's) and digital-to-analog converters (DAC's), respectively. The Penn State ED ANC system consisted of a Motorola 96002 DSP, capable of 16.5 MIPS or 49.5 MFLOPS (peak) with a 33 MHz clock. That system also provided 32 input channels and 16 output channels for the DSP, with 12-bit ADC's and DAC's.

5.3.2 Signal Conditioning

In order to make the most efficient use of the ADC's and DAC's, the analog signals routed to and from the I/O board need to be scaled properly. This is accomplished by the signal conditioning electronics. Adjustable gain can be applied to each of the six microphone signals from the error sensor. A gain of 0, 10, or 20 dB can be applied to all six signals simultaneously, or each signal can be fine tuned with a multi-turn potentiometer. Individual adjustment of each input channel allows the ED sensor to be calibrated and for any sensitivity mismatch in the microphones to be compensated for. Manual adjustment of the output gains is also available for the control signals being routed to the satellite speakers and subwoofer. All analog signals are low pass filtered before the ADC's to reduce the risk of aliasing, and immediately following the DAC's to eliminate undesired high frequency content due to quantization.

The reference signal passes through a programmable frequency multiplier, that will allow recorded (or real) tachometer signals to be used directly as the reference input.

This is important, since a tach signal will sometimes be at the engine rotation speed, which is some fraction of the firing frequency. Tach signals can also be at a frequency many times the firing frequency. In either case, the programmable frequency multiplier can produce the appropriate reference signal. The option to bypass the frequency multiplier is provided with a toggle switch.

After the control signals pass through the low pass smoothing filters, they enter the crossover circuitry. The crossover circuitry produces output signals for the satellite speakers by high pass filtering the control signals with a 90 Hz cutoff frequency. For the subwoofer signal, the two control signals are summed and then low pass filtered at 90 Hz. All control signals are then fed to a power amplifier, which drives the loudspeakers directly. A photo of the electronics appears in Figure 5.7.

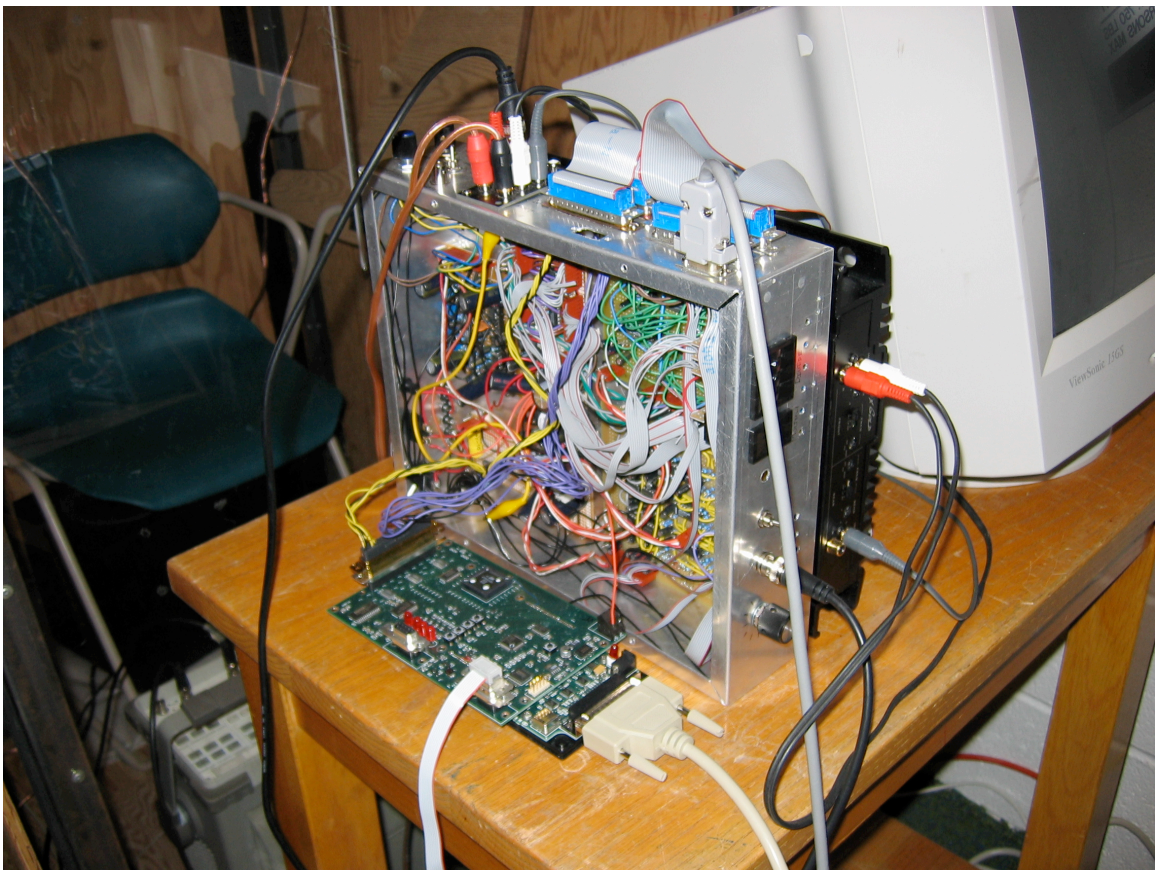

Figure 5.7 ANC system electronics.

5.4 Instrumentation

In order to determine the global nature of the noise control, as many as 15 microphones measured the sound pressure inside the mock cab at one time. All but three of these microphones were arranged in two horizontal planes containing six microphones each. These two planes were chosen to be located above and below the ear level of the operator, and extended from the back to the front of the mock cabin. Two other microphones were strapped to a set of headphones, worn by the operator inside the cab, to measure sound pressure levels near the operator's ears. The headphones provided a convenient method for mounting the microphones near the operator's ears and also allowed for instructions to be easily communicated to a person in the cab during experiments. For most measurements reported in Chapter 6, when an operator was not sitting in the cab, the headphones were suspended from the ceiling of the cab in essentially the same location as they would be when worn by the operator. In this case, a Styrofoam block was placed between the ear pieces. The fifteenth microphone was actually one of the microphones inside the ED sensor, where the maximum level of attenuation was likely to be found. These microphones were routed to the inputs of a 48-channel SignalCalc 620 Dynamic Signal Analyzer from Data Physics Corporation. A photo of the numerous microphones appears in Figure 5.8.

For static measurements, in which the frequency of the noise and reference signal did not change, the SignalCalc 620 system was used to obtain time-averaged power spectra from all the microphones, with the ANC system both on and off. In the case of dynamic measurements, in which the tonal noise changed in frequency, several signals were streamed to disk, with a 44.1 kHz sampling rate, for post processing. These signals

included that of a single error sensor microphone, the 2 “ear microphones,” and 4 of the additional 12 microphones located in the upper plane nearer the front of the cab. Those four microphones were chosen to monitor noise levels furthest from the error sensor, but in the region where the operator’s head was most likely be if the operator leaned forward.

Figure 5.8 Microphones used to measure the performance of the ANC system.

CHAPTER 6

MEASUREMENTS AND RESULTS

6.1 System Identification

As discussed in Chapter 4, the process of system identification (SysID) enables proper operation of the filtered-x adaptive algorithm—the heart of the control system. The net result of SysID is a set of digital filters, representing the impulse responses of the various components of the secondary signal path(s), which are convolved with the reference input signal to produce the filtered-x signals. The accuracy of the SysID filters, or models, depends on such system variables as input and output signal gains, sampling rate, and filter length. For the measurements discussed below, all signal gains were adjusted to allow for maximum use of the full scale voltage range of the ADC's and DAC's, with some headroom to prevent clipping.

6.1.1 Sampling Rate Versus Filter Length

In order to gain a better understanding of how the quality of the SysID filters depends on sampling rate and filter length, the minimum mean square error (MMSE) between the output of the SysID filters and the output of the true secondary path was found as a function of sampling rate and filter length. This MMSE was determined according to Equation 4.23. Figures 6.1 and 6.2 display the MMSE for one component of the particle velocity path and the pressure path, respectively.

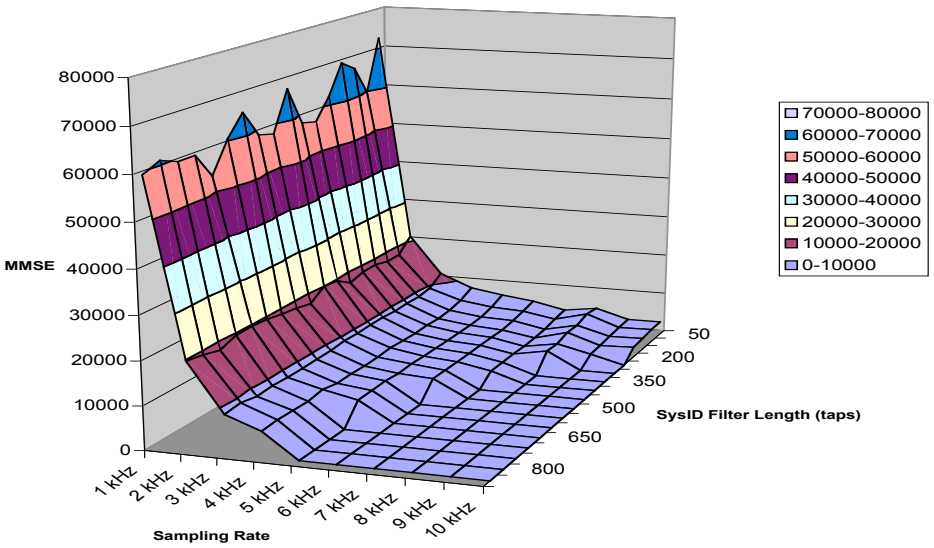

Figure 6.1 Velocity path model MMSE

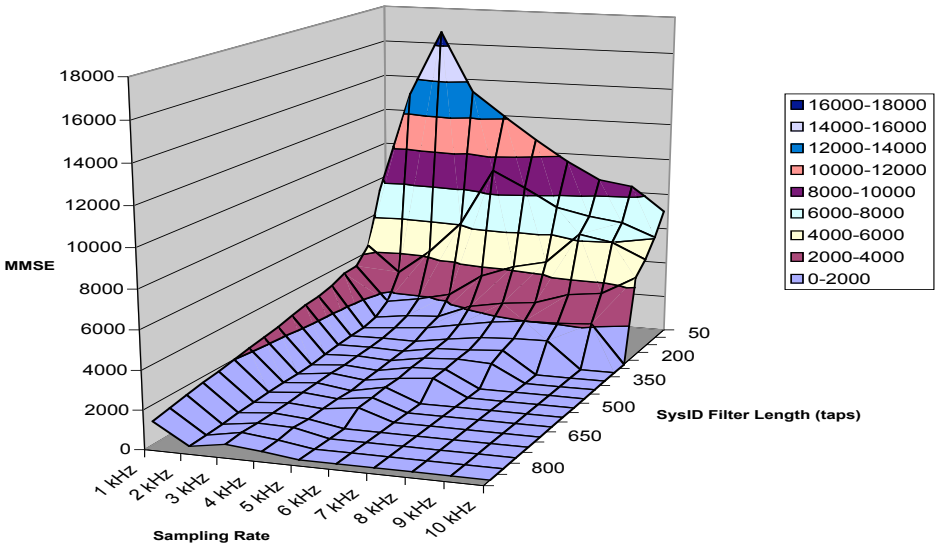

Figure 6.2 Pressure path model MMSE

Figure 6.1 shows a strong dependence on sampling rate for the MMSE obtained for the velocity path. Minimum error in particle velocity path estimate was expected to have some dependence on sampling rate due to the integration over time required to obtain particle velocity from pressure measurements. This integration is performed as a summation in the DSP, so the higher the sampling rate, the smaller the time difference

between samples, and the more closely the algorithm approximates a true integral. However, increasing the filter length did not have a significant impact on the error. The pressure path behaves in essentially the opposite manner, as shown in Figure 6.2. It does not show a strong dependence on sampling rate, but the error does decrease with filter length; although the slope of the error with respect to filter length is not as steep beyond two or three hundred taps (coefficients).

In order to explore the effects of the quality of the SysID filters on actual control system performance, the control system attenuation of tonal noise with a fixed frequency using SysID filters of various lengths, and at various sampling rates, was measured. The results are displayed in Figure 6.3. Performance of the control system when attenuating a 50 Hz tone showed very little dependence on the length of the SysID filters. However, for higher sampling rates, the shortest filters (50 taps) prevented the system from converging at all. There was some dependence on sampling rate, but performance appeared to level off above 3 kHz sampling. These results suggest that increasing the sampling rate or SysID filter lengths will not necessarily improve performance. This agrees with Snyder's[18] contention that a faster, more powerful DSP processor will not solve all problems with ANC. However, the new ANC system with its faster DSP enabled the exploration of longer filter lengths and higher sampling rates than were possible with the older Motorola DSP.

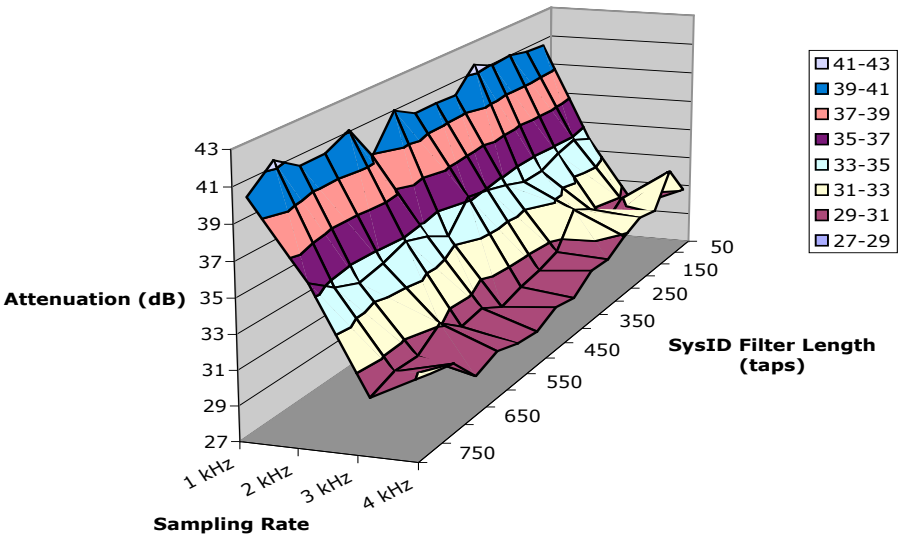

Figure 6.3 Attenuation of a 50 Hz tone using ED ANC.

Following the fixed-frequency measurements, a variable frequency excitation signal was created to provide noise inside the mock cab, as well as a reference input to the ANC system. A sinusoid was swept in frequency between 40 and 120 Hz at two different speeds. The test signal itself consisted of four sections. The first consisted of sweeps lasting for three seconds with the end frequencies held for three seconds before the swept sine reversed direction. In the second section, the frequency swept up and down at the same rate without being held at either end (40 or 120 Hz). The last two sections were similar in nature to the first two, except that the frequency was swept for 0.5 seconds in each direction and the end frequencies were held for 1 second. A spectrogram of the signal is shown in Figure 6.4.

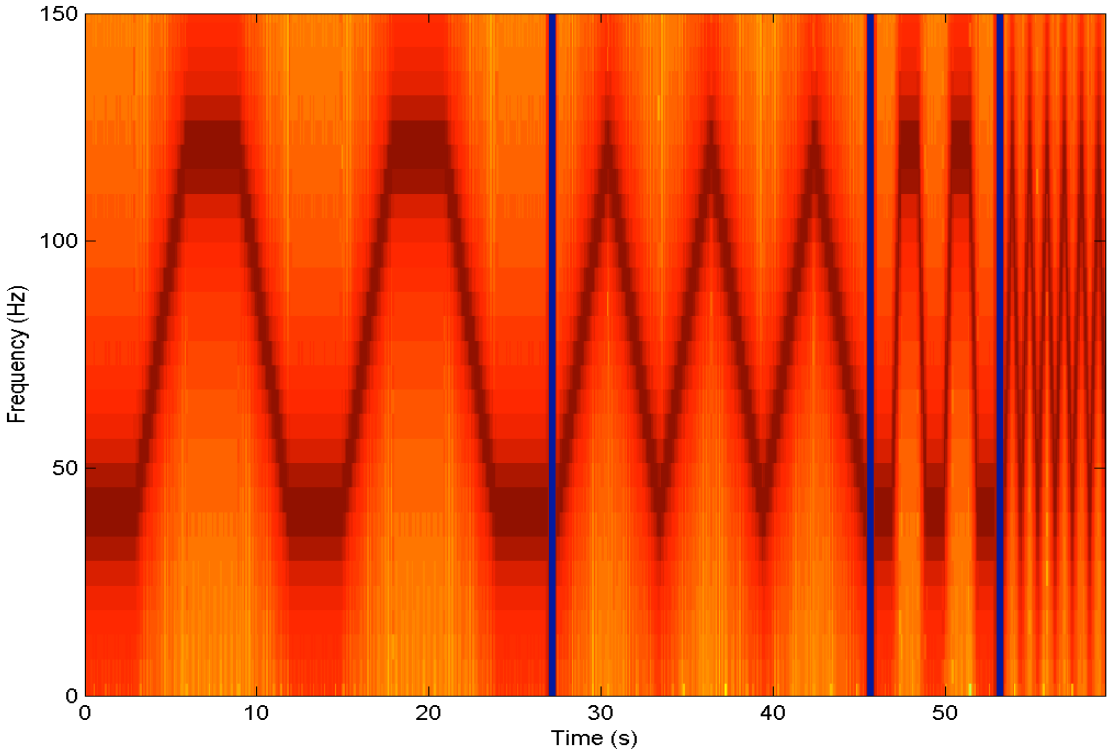

Figure 6.4 Swept sine excitation signal for studying the dependence of dynamic ANC performance on SysID parameters.

At a sampling rate of 2 kHz, various SysID filter lengths resulted in varying performance values for the ANC system. The performance was measured by subtracting the equivalent sound level (L_{eq}) over the duration of the excitation signal with the control system running from the L_{eq} obtained over the same duration with the control system off. Figure 6.5 displays the results obtained with 5 different filter lengths. A filter length of 20 taps was too short (at the chosen sampling rate) to enable the control system to function well, and the result was a higher L_{eq} than with no control at all. Beyond 60 taps, however, the control system performance did not improve significantly (in this particular test, 100 taps provided the best result). A clue about the reason for this performance plateau comes from the impulse response of the secondary path (which is exactly what the SysID filters try to model). A plot of the squared impulse response can be seen in

Figure 6.6. Much of the energy in the impulse response is contained within the first 80 milliseconds, which suggests that a filter should have enough coefficients to represent the first portion of the response, but beyond a certain length corresponding to that time, little is gained. In fact, beyond that point, the performance can often degrade, due to factors such as misadjustment error.[16]

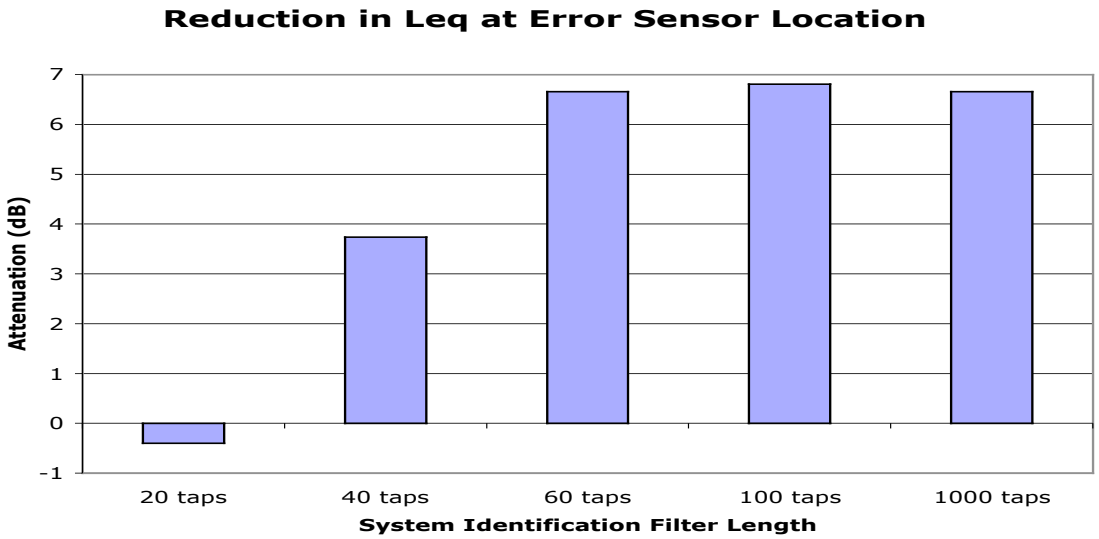

Figure 6.5 ANC performance dependence on SysID filter length. The sampling rate for this measurement was 2 kHz and a single control channel was used.

At a sampling rate of 2 kHz, 20 taps in a SysID model corresponds to 10 ms of the impulse response. This is not enough to capture the main peak in the impulse response, which could explain the poor performance of the system with such a short filter. The filter with 40 taps, however, was just long enough to capture some of the main peak, but not what appears to be a significant amount of information following that peak. Its performance was not as good as the longer filters that were able to capture additional information (including the second largest peak). However, stretching the filters out to 1000 taps (0.5 seconds of the impulse response), yielded no improvement over filters which captured a mere 50 ms of the impulse response.

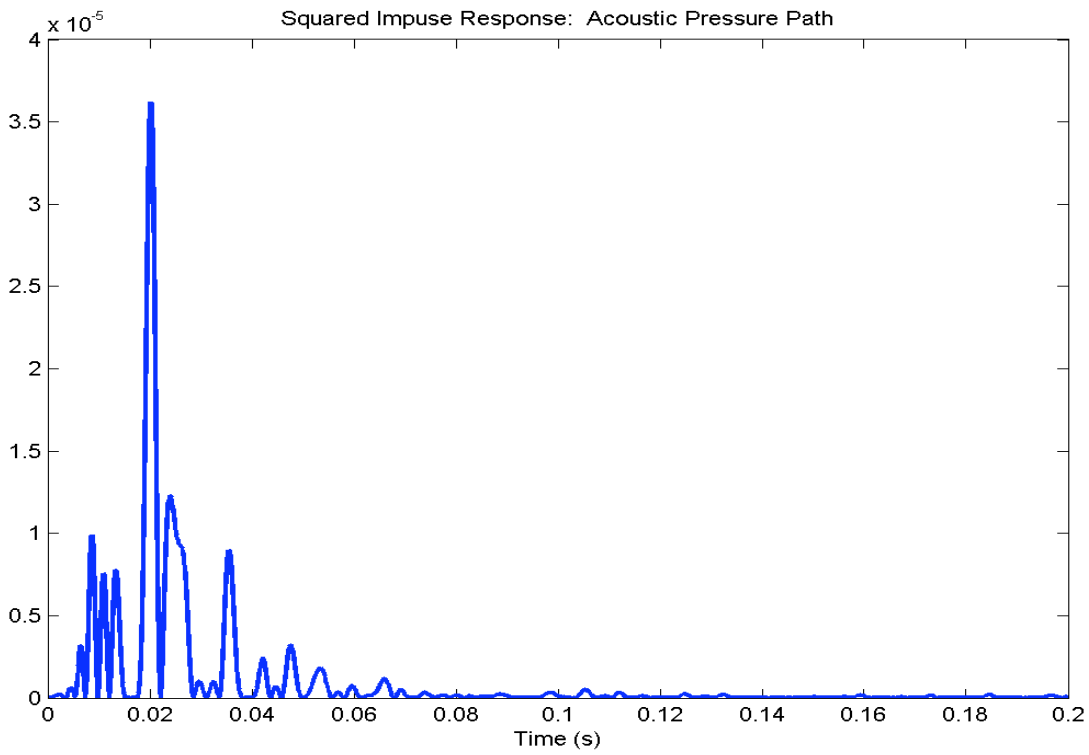

Figure 6.6 High resolution squared impulse response for the acoustic pressure path, measured with the cab door closed. The sampling rate for this measurement was 96 kHz.

It should be noted that these results are for tests involving many frequencies, where a broadband SysID filter is required. If steady state pure tones are used, it is not necessary to match the full impulse response, since the SysID filter is only required to get the proper magnitude and phase response at a single frequency, which can be accomplished with a minimum of two coefficients. As far as bandwidth is concerned, the SysID filter must be valid over the frequency range in which the control system is intended to operate. This requirement should be met as long as the sampling rate of the DSP is more than twice the cutoff frequency of the antialias filters for the error sensor and reference signal. The electronics, including the ED sensors, were designed to allow frequencies up to 400 Hz to be controlled. However, experiments conducted in this research were conducted for tonal noise frequencies up to 200 Hz. In the event that

future research efforts explore the control of additional types of noise within a tractor cab, including higher harmonics of the engine firing frequency, the maximum control frequency of 400 Hz will likely be beneficial.

To investigate the dependence of the control system performance on sampling rate, similar tests were conducted with sampling rates of 1 kHz and 4 kHz. The chart in Figure 6.7 demonstrates a comparison of reductions in L_{eq} for several sampling rates and filter lengths. Each color in the graph represents a different sampling rate. The best of the results shown in Figure 6.5 was chosen to represent the performance with a 2 kHz sampling rate. Results were obtained for the 1 kHz and 4 kHz sampling rates with the same filter length, and then with filter lengths that captured the same amount of the impulse response (50 ms) as that for the 2 kHz case. Performance in the 2 kHz case was superior to that obtained with either of the other sampling rates.

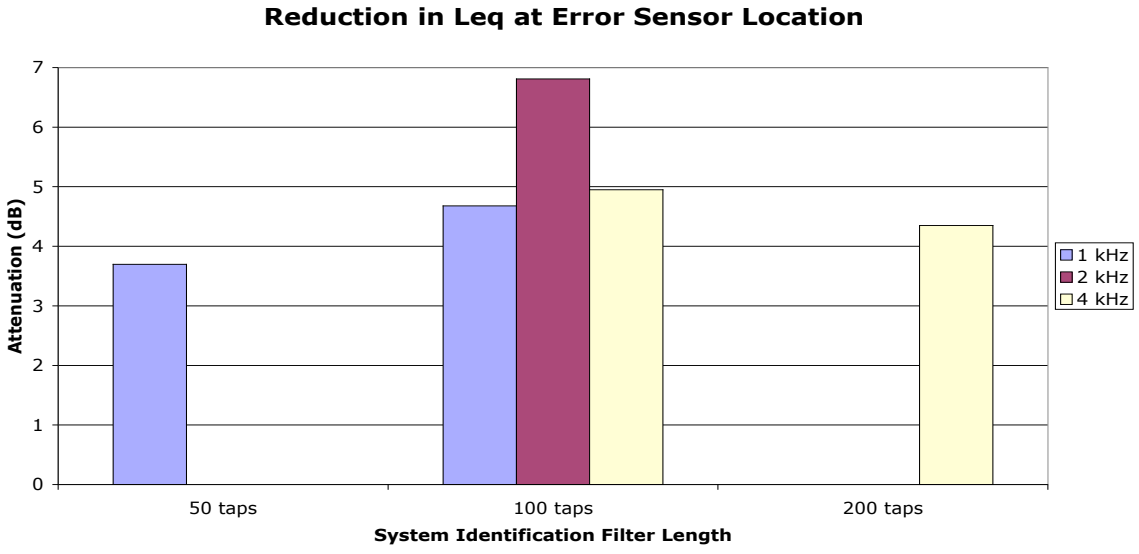

Figure 6.7 ANC performance dependence on sampling rate. A single control channel was used in these measurements.

6.1.2 SysID and Stability Issues

Since the research currently being discussed used offline SysID almost exclusively (see Chapter 4), some work was undertaken to understand the implications of using linear time-invariant (LTI) SysID models in a time-varying system. Some possible changes to the actual system that might be encountered in the target application of this control system were considered. SysID measurements were performed with the cab door open and closed, with the subwoofer control speaker in two locations, and at various temperatures. Three squared impulse response magnitudes are displayed in each of Figures 6.8 and 6.9, which correspond to the pressure and velocity paths, respectively.

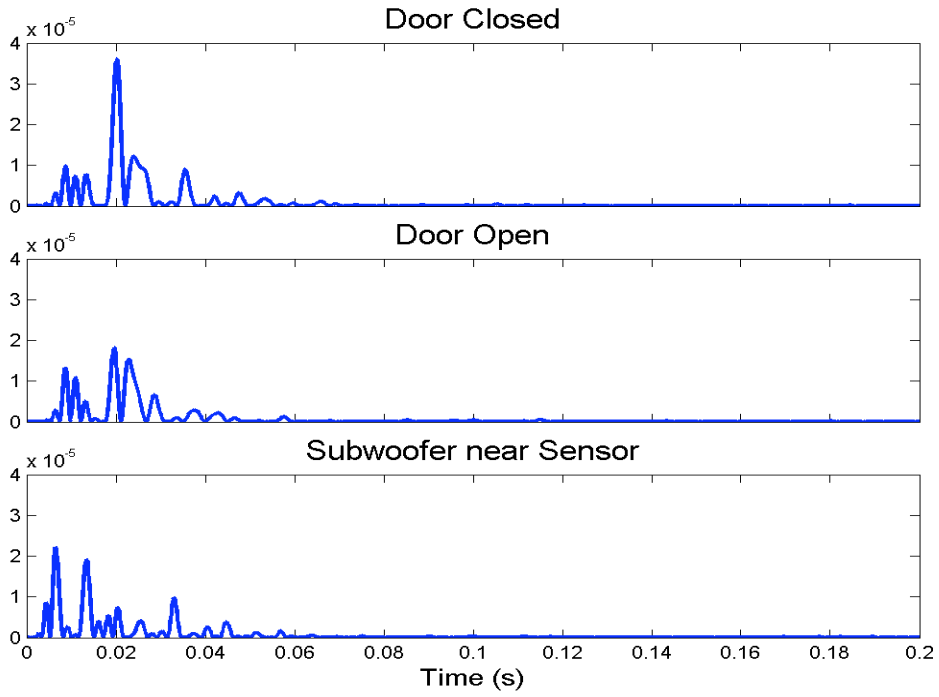

Figure 6.8 Pressure path squared impulse response magnitudes. The MMSE was on the order of 10^{-4} for pressure.

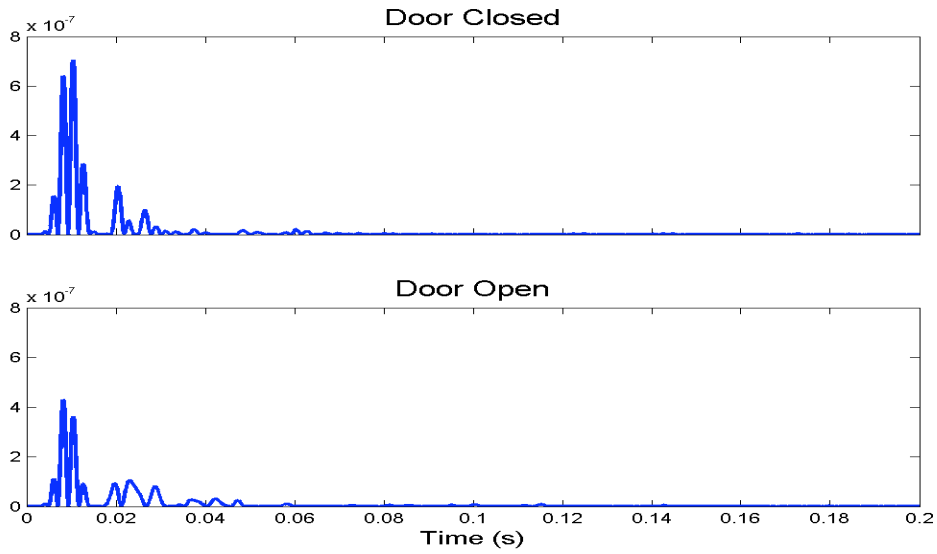

Figure 6.9 Particle velocity path squared impulse response magnitudes. The MMSE was on the order of 10^{-6} for particle velocity.

The impulse response curves for the two cases of cab door open and cab door closed appear very similar except for the different amplitudes of the respective peaks. This is true of both the pressure as well as the particle velocity paths. However, the impulse response obtained with the subwoofer placed on the chair, much closer to the error sensor than where it is shown in Figure 5.1, is significantly different than the other two. A significant portion of the energy in the impulse response is shifted earlier in time, which is to be expected due to the reduction in the propagation time of the acoustic signal between the subwoofer and error sensor.

For comparison, the impulse responses obtained at three different temperatures are shown in Figure 6.10. These impulse responses are virtually identical, which suggests that temperature is not likely to significantly impact ANC system performance in an actual tractor cab.

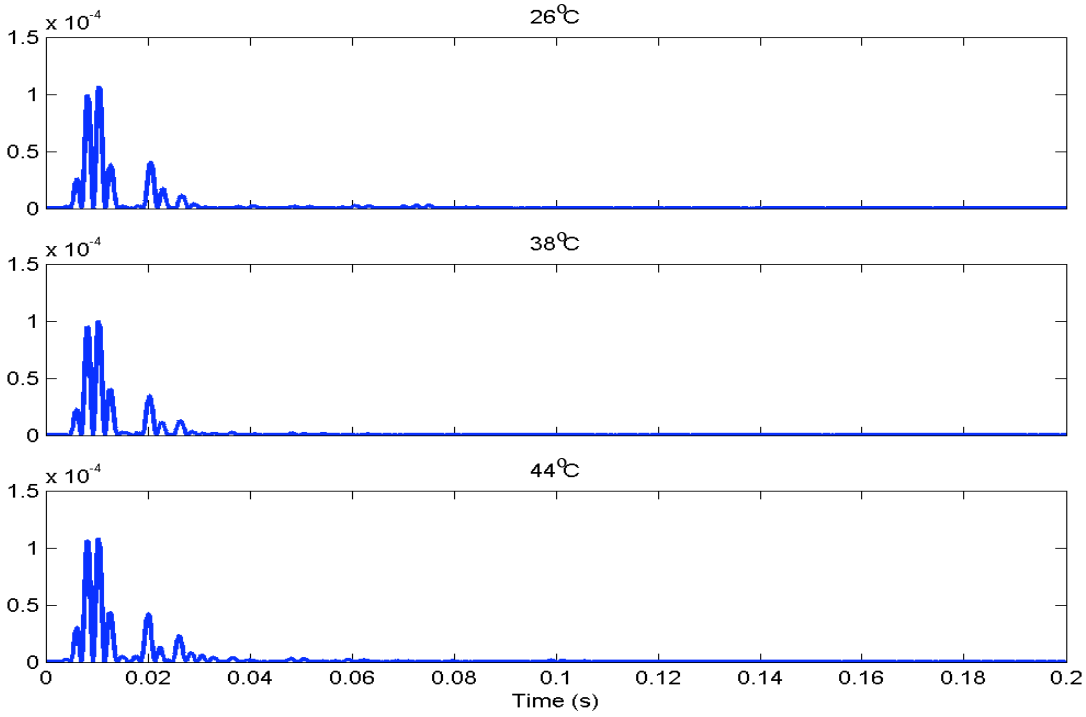

Figure 6.10 Particle velocity impulse response comparison at three different temperatures. These responses were obtained with the cab door closed.

Figure 6.11 displays the results comparing the reduction in L_{eq} achieved with SysID filters obtained in the conditions just described. For these measurements, the cab door was closed and the system was run at a temperature of 26 ºC, using the SysID filter coefficients obtained at the various temperatures or cab configurations. As suggested by the impulse response curves, the variations in temperature, from the time the SysID filter coefficients were obtained, did not significantly impact the control system performance. The SysID filters obtained at 44 ºC did yield slightly less reduction of the L_{eq}, however. The system did not become unstable using the open door SysID filters, but the performance was noticeably reduced. The only case that caused stability problems was having one of the control speakers, the subwoofer, closer to the error sensor when offline SysID was performed than when the control algorithm was run. These results support the idea that one of the most important parameters for the successful operation of the ANC

system is the initial time delay through the secondary path. The range of temperatures likely to be encountered in an actual tractor cab, along with typical dimensions of such a cab, appear to be such that the change in the initial time delay, as a function of temperature, is insignificant.

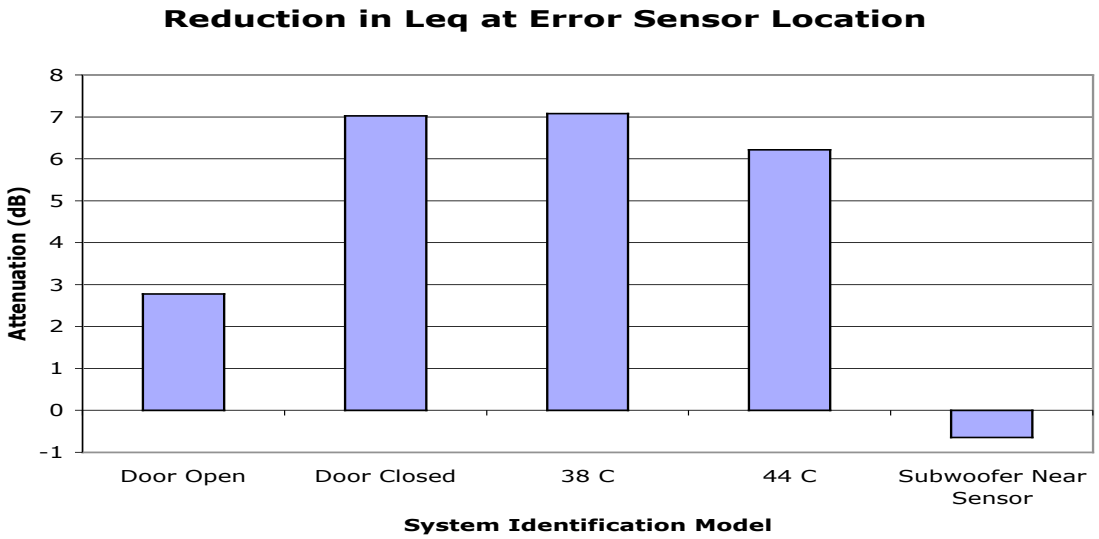

Figure 6.11 ANC performance using SysID filters that may not accurately model the current secondary path.

One additional test performed to check stability of the system with regard to SysID models was to move the mock cab from the large hallway where it normally rests into an anechoic chamber. For many of the frequencies of interest, however, the anechoic chamber was as resonant as the hallway, which exhibits strong modes near 50 and 60 Hz. The anechoic chamber at Brigham Young University ceases to be anechoic below approximately 70 Hz. The results just discussed actually involved SysID filters obtained with the cab in the hallway, but the control was run inside the anechoic chamber. The results were actually quite similar to those obtained in the hallway, so moving the cab into the chamber did not change the system enough to significantly degrade system performance.

6.2 Static System Performance

The static performance of the ANC system was measured at several fixed frequencies by the array of microphones described in Chapter 5. Initially, the control system was operated using a single frequency coming from a signal generator, which was used to drive the noise source as well as to provide the reference input. An additional set of measurements reveals the performance of the control system when recorded steady noise from an actual tractor engine is broadcast into the mock cab and a tachometer signal from the engine is used as the reference input. Several plots follow, which compare the tonal attenuation achieved by the ANC system at various frequencies. Also compared in the plots are performance values for ED and SP-based control in dual and single control channel configurations. In the single channel configuration, only a single control filter was implemented in the DSP and the output of that filter was sent to both satellite control speakers, rather than just one of them. The measurements involving recorded tractor noise only employed 2-channel control. In all cases the control system was run with a sampling rate of 2 kHz, control filters with 32 coefficients, and SysID filters with 300 coefficients (300 was the ANC system's default SysID filter length).

6.2.1 Static Attenuation of Single Tones

The following three figures, Figure 6.12 through Figure 6.14, show the attenuation achieved by the control system at seven discrete frequencies. These frequencies were chosen so that several of them corresponded to the predicted modal frequencies of the mock cab (Figures 5.2-5.5). The chosen frequencies were 50, 80, 113, 125, 154, 171, and 195 Hz. Additional performance measures of the control system at 50 Hz can be seen in section 6.1.1. Single channel control was not run at 50 Hz.

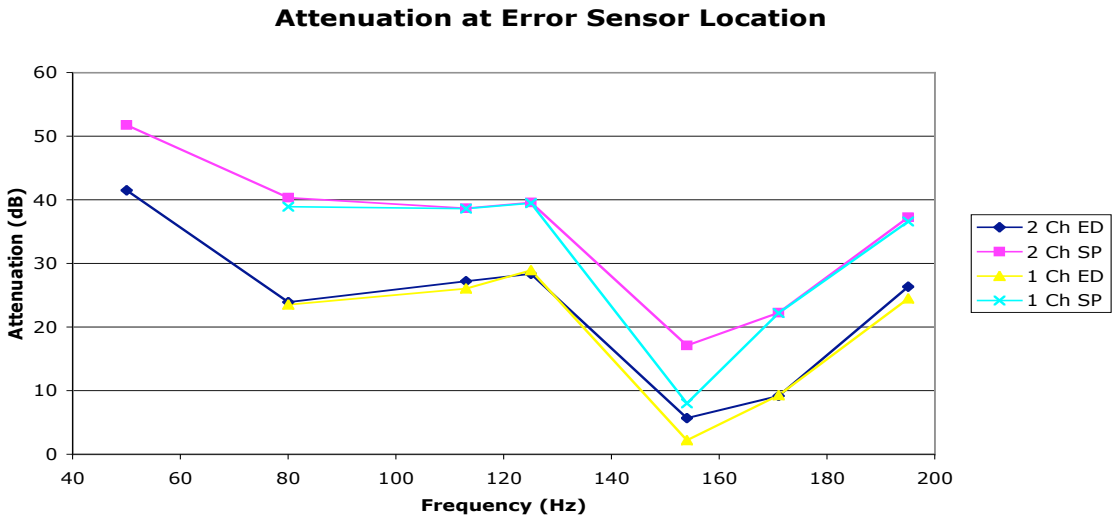

Figure 6.12 Attenuation of various tones, measured at the error sensor, comparing ED and SP control in 1 and 2-channel control configurations.

As shown in Figure 6.12, minimizing squared pressure provided superior attenuation at the error sensor, even for the single-channel case. Minimization of ED provided significant amounts of attenuation, but that attenuation was generally 10 dB less than that obtained with the SP-based control. The single control channel performed nearly as well as the two-channel control configuration in almost all cases.

At the microphones near the operator's ears (the ear microphones), the SP control still outperformed the ED control at the lowest frequencies. This can be seen in Figure 6.13. A the higher frequencies, above the crossover frequency between the subwoofer and satellite control speakers, the ED control provided the best attenuation. At these higher frequencies, there is more of a modal response in the cab, and it is at these frequencies where ED control is expected to perform better. At the lowest frequencies, there is no real modal response in the cab, so the SP control is expected to perform at least as well as the ED control. At 154 Hz, the SP control actually produced a higher noise level at the operator's ears than existed without control, presumably due to the

proximity of the nodal region in the mode that exists near 154 Hz. The SP error sensor probably had difficulty observing the noise in the cab at that frequency. Again, for SP control the single and dual channel configurations provided nearly identical results. For ED, however, the single channel case actually provided significantly better attenuation at 113 Hz, but in general the dual channel control provided the best performance by at least a small margin.

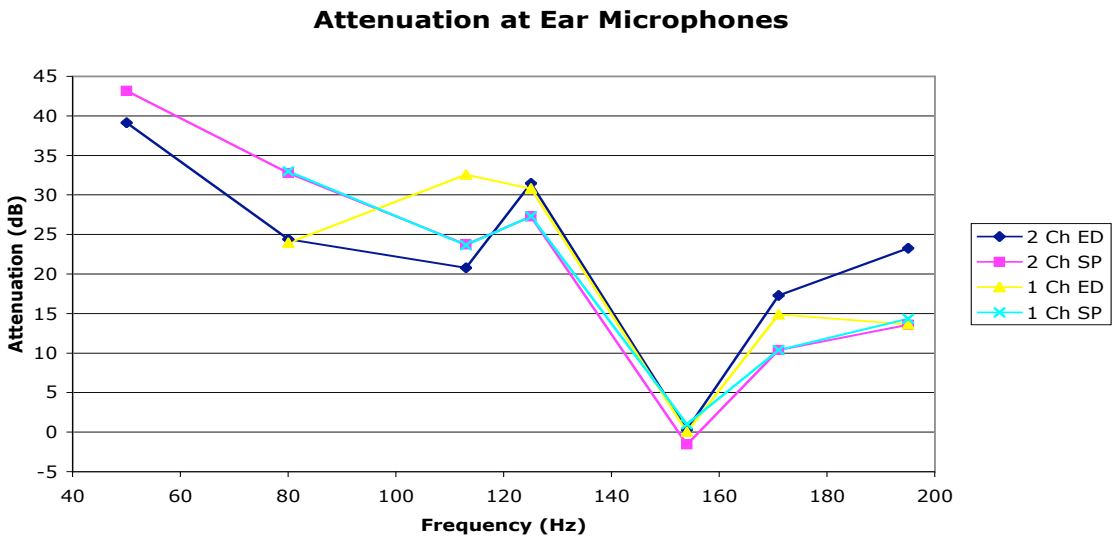

Figure 6.13 Attenuation of various tones, measured at the ear microphones, comparing ED and SP control in 1 and 2-channel control configurations.

A spatial average over the 12 distributed microphones in the cab provided a global performance measurement. At most frequencies, all control configurations yielded similar levels of attenuation, as shown in Figure 6.14. At 154 and 171 Hz, ED control outperformed SP control, even though all configurations produced a net increase in the average noise level at 154 Hz. The lesser performance at the highest 3 frequencies, especially at 154 and 171 Hz, might have been predicted based on the mode shapes for the mock cab shown in Chapter 5. The error sensor was positioned inside the nodal region for the mode near 171 Hz, shown in Figure 5.4. The sensor was also quite close to

the nodal region for the second mode of the cab, shown in Figure 5.3. The nodal structures at these frequencies suggest an observability problem for a pressure sensor, but not necessarily for an energy density sensor.

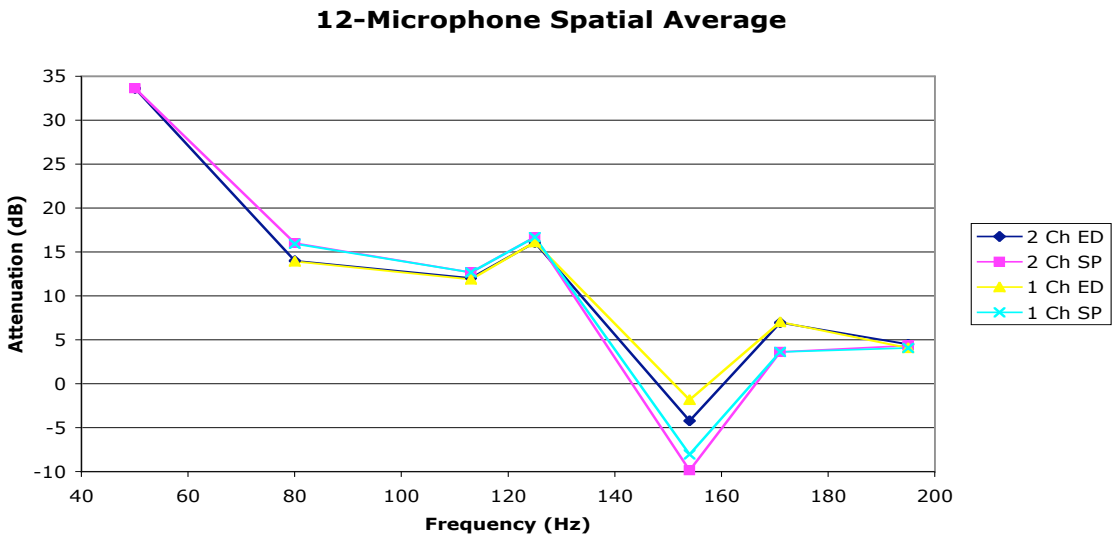

Figure 6.14 Attenuation of various tones, averaged over 12 distributed microphones, comparing ED and SP control in 1 and 2-channel control configurations.

6.2.2 Static Attenuation of Recorded Tractor Noise

Tractor noise recordings were made at four different engine speeds, and those recordings were played back inside of the mock cabin in order to test the control system. A tachometer signal was recorded as well and was routed to the reference input of the ANC system electronics. A toggle switch routed this signal through the aforementioned programmable frequency multiplier, which converted the signal into an appropriate reference signal for the filtered-x control algorithm. The desired reference signal was a sinusoid at the engine firing frequency for each of the recordings. The frequency multiplier circuitry provided a square wave signal at the appropriate frequency, and the signal was then low-pass filtered to reduce undesired harmonics. The four recordings captured engine firing frequencies of roughly 41, 91, 99, and 117 Hz.

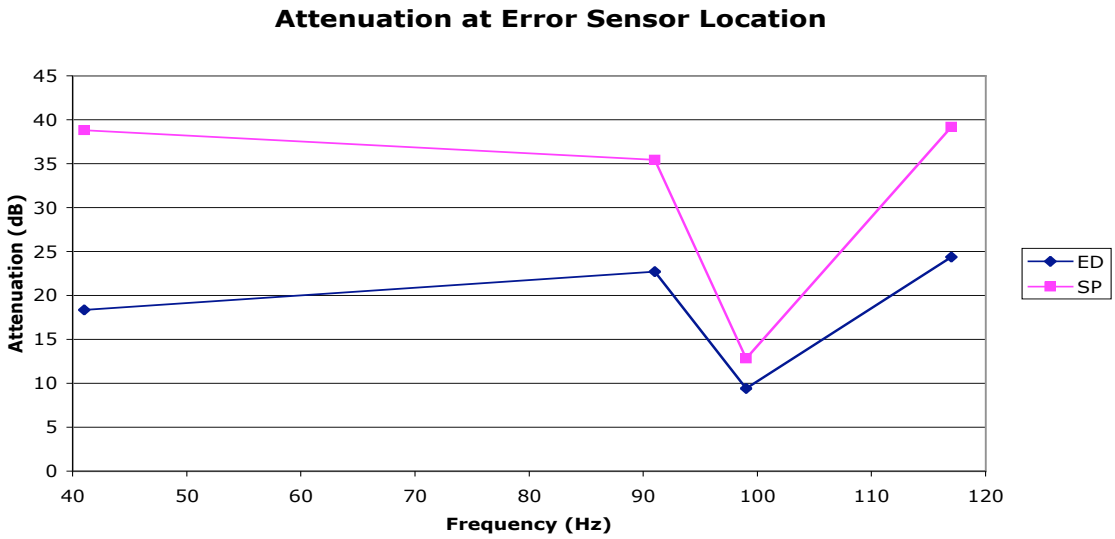

Figure 6.15 Attenuation of tractor engine tones, measured at the error sensor, comparing ED and SP control in a 2-channel control configuration.

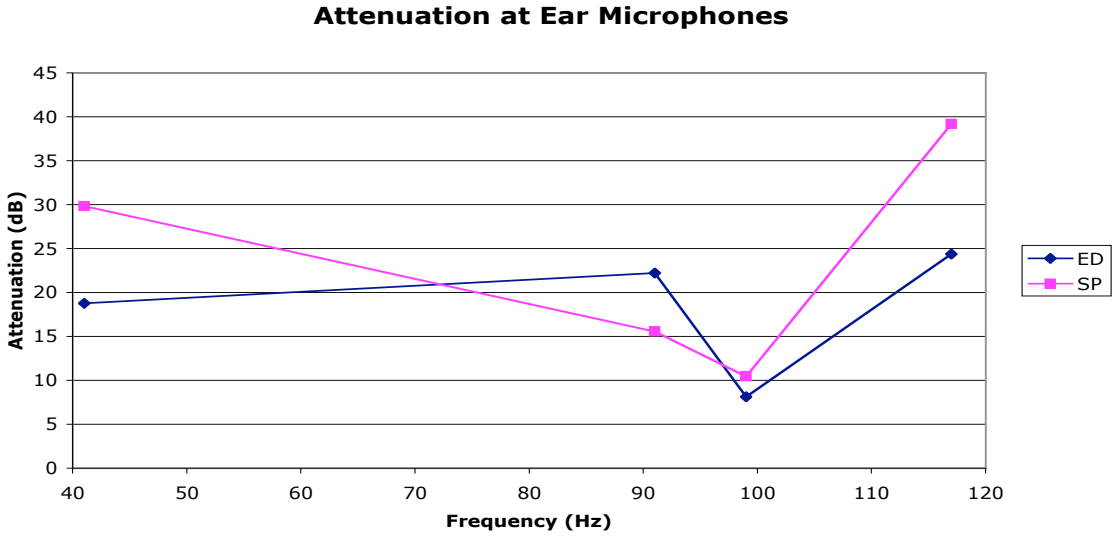

Figure 6.16 Attenuation of tractor engine tones, measured at the ear microphones, comparing ED and SP control in a 2-channel control configuration.

Similar to what was seen with the synthesized sinusoid, Figure 6.15 shows that the SP control outperforms the ED control at the error sensor. Figure 6.16 shows a narrowing of the gap between the two control systems when observed at the operator's head position, with the ED control providing better attenuation near the operator's head at

91 Hz. For the global measurement, shown in Figure 6.17, the SP control continues to provide superior attenuation, but the differences are essentially insignificant.

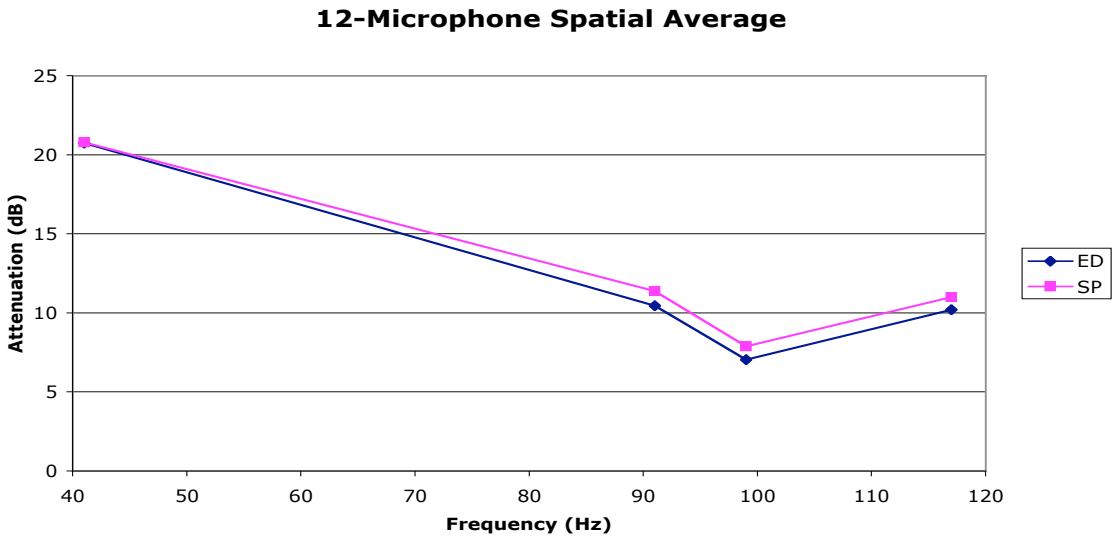

Figure 6.17 Attenuation of tractor engine tones, averaged over 12 distributed microphones, comparing ED and SP control in a 2-channel control configuration.

6.3 Dynamic System Performance

Control system performance for attenuation of a frequency varying tone was also measured using a synthesized excitation signal, as well as recorded noise due to tractor engine speed sweeps. Dynamic performance measurements were made in order to compare ED and SP-based control. These measurements were performed in single and dual channel control configurations, except when recorded tractor noise was used, in which case only a dual channel control configuration was used. Again the system was operated with a 2 kHz sampling rate, 32-tap control filters, and 300-tap SysID filters. The performance measure was the achieved reduction in L_{eq} over the duration of the excitation signal. The equivalent sound level was measured by 1 of the error sensor microphones, the 2 ear microphones and 4 of the 12 distributed microphones. The reason

for the reduced microphone count was the need to stream all data to hard disk for post processing, which proved to be difficult with the SignalCalc 620 system. An 8-channel hard disk recording system provided a simpler means for obtaining the desired data. The microphones used were those nearest the top of the cab and closest to the front.

One parameter of the ANC algorithm that can drastically affect the performance of the system in dynamic conditions is the step size, μ, of the adaptive filter. Generally, decreasing μ in an adaptive filter decreases the residual error in the filter after it has converged. However, decreasing μ also slows the rate at which the filter converges. In the static measurements, no appreciable performance gain was achieved by making μ smaller as long as it was small enough to ensure stability of the ANC algorithm. Therefore, for the dynamic measurements discussed below, the step size was kept as large as possible to enable the ANC system to adapt quickly without becoming unstable. Generally, for the system being discussed, μ is on the order of 10^{-10} for both ED and SP-based control in single as well as dual-channel control configurations.

6.3.1 Dynamic Attenuation, Swept Sine Excitation

The swept sine excitation signal used to obtain the results that follow exhibited similar characteristics to the signal described in section 6.1.1. The upper frequency was 200 Hz, rather than 120 Hz; the slow sweeps had a duration of four seconds with the end frequencies held for four seconds; and the fast sweeps had a duration of one second with the end tones held for one second. A spectrogram of the signal appears in Figure 6.18.

The performance of the system was evaluated for the entire test signal as well as for each of the individual sections of the test signal. Figures 6.19 and 6.20 show that at the error sensor and ear microphone locations, the 2-channel ED control provided the

greatest reduction in L_{eq}, followed by the 1-channel SP control. This was true for the entire duration of the test signal as well as for the portions including slower sweeps.

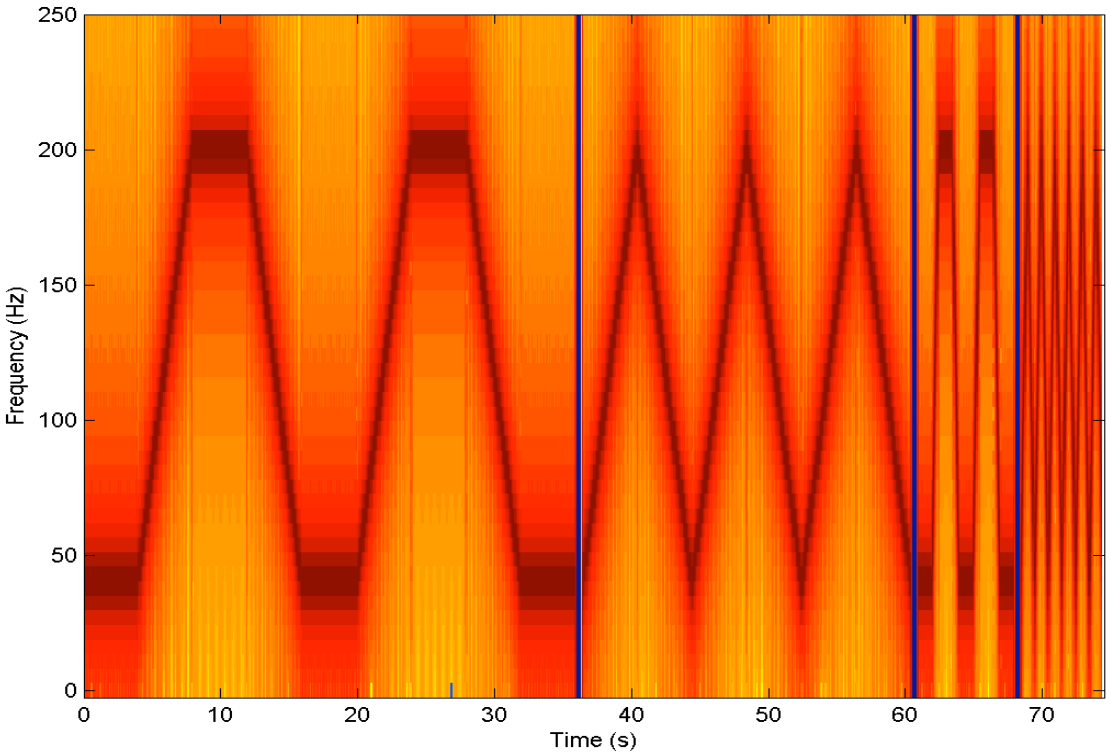

Figure 6.18 Swept sine excitation signal for studying dynamic ANC performance.

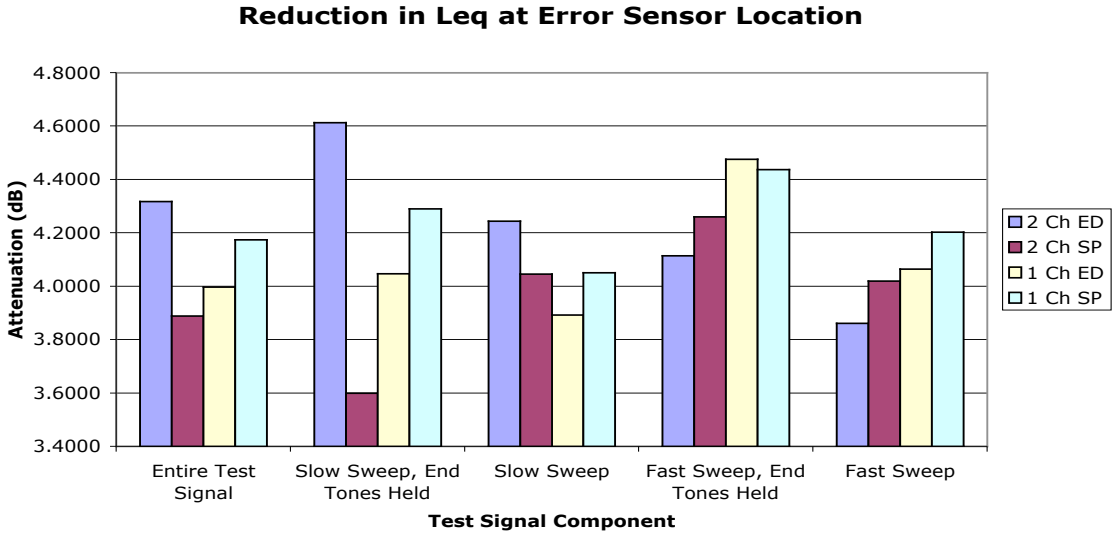

Figure 6.19 ANC system reduction of L_{eq} at the error sensor. These results were obtained with the control system operating at 2 kHz with 300-tap SysID filters.

For the faster sweeps, the single channel ED and SP control configurations narrowly outperform the dual channel cases. Performance differences for the 4-microphone spatial average were much smaller as shown in Figure 6.21.

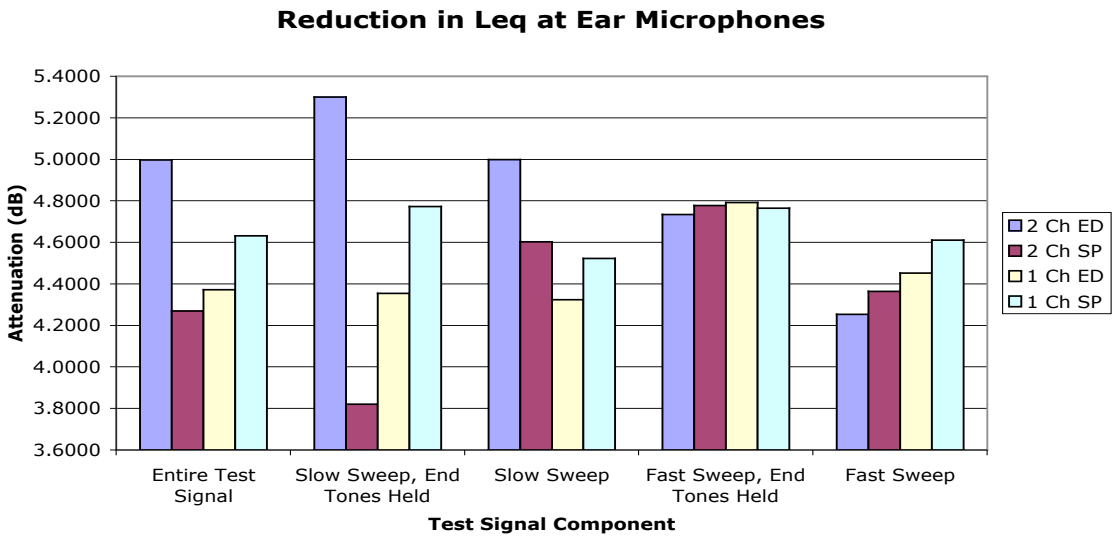

Figure 6.20 ANC system reduction of L_{eq} at the ear microphones. These results were obtained with the system operating at 2 kHz with 300-tap SysID filters.

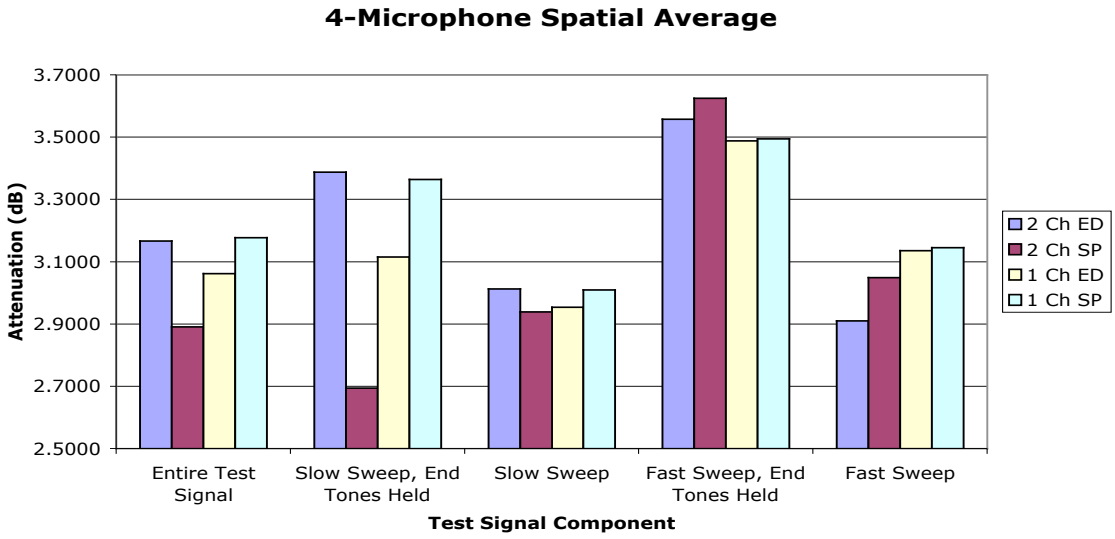

Figure 6.21 ANC system reduction of spatially averaged L_{eq}. These results were obtained with the system operating at 2 kHz with 300-tap SysID filters.

Figure 6.22 contains time-averaged spectra measured by the left ear microphone without ANC, with ED control and with SP control. There are clearly some regions of

the spectrum where the ANC system provided significant levels of attenuation, but in the region between 70 and 110 Hz, the noise level was actually increased somewhat. However, the noise level between 70 and 110 Hz without control is noticeably lower than frequencies above and below that range, so one would expect that the subjective effect with a varying frequency would be improved with the implementation of ANC.

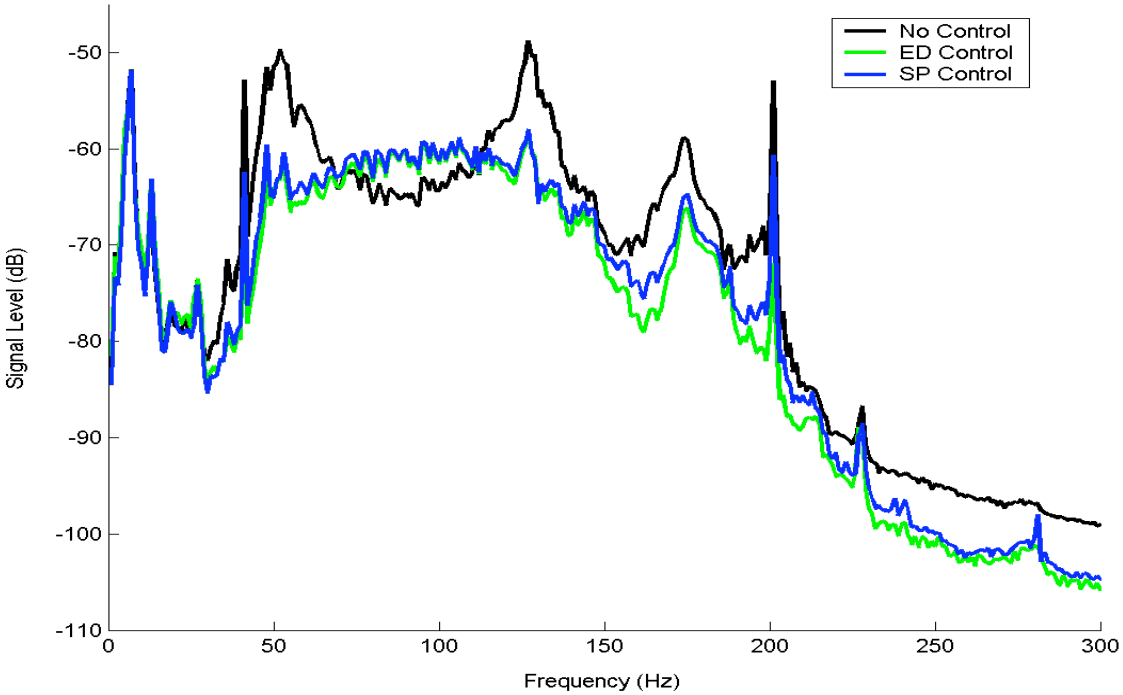

Figure 6.22 Time-averaged spectrum of swept sine excitation signal measured with and with out ANC by the left ear microphone.

6.3.2 Dynamic Attenuation of Recorded Tractor Noise

Three recordings of tractor engine noise were used to measure the dynamic ANC performance in the hopes of closely reproducing what might be achieved by placing the control system in an actual tractor. Each of the recordings contained engine speed sweeps that varied the engine speed from its lowest to its highest limits. Three sweep rates were recorded, one rate for each recording. The slowest rate was significantly slower than that of the synthesized frequency sweeps discussed previously. However, the

medium engine speed sweep rate was comparable to the slow synthesized frequency sweep rate and the fastest sweep rates for the tractor noise and synthesized excitation signal were comparable as well. The engine firing frequency stayed between 40 and 120 Hz. This is the only set of measurements for which a person was actually sitting in the mock cab while the control system was run. Figures 6.23 through 6.25 show the results for the dynamic tractor noise measurements.

All three measurement locations yielded very similar results. SP control marginally outperformed ED control for the slow sweeps, but fell behind for the faster speed sweeps. In fact, when the engine speed was swept at the fastest rate, the SP control resulted in a higher L_{eq} than was present with no control, but the ED control always provided some attenuation.

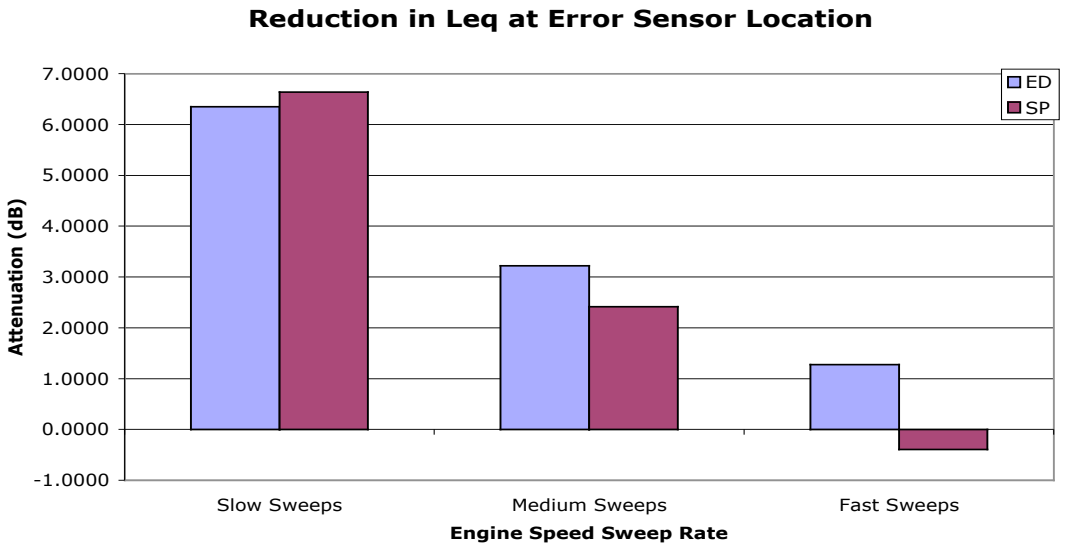

Figure 6.23 ANC system reduction of L_{eq} at the error sensor. These results were obtained with recorded tractor noise as the excitation signal and the control system operating at 2 kHz with 300-tap SysID filters.

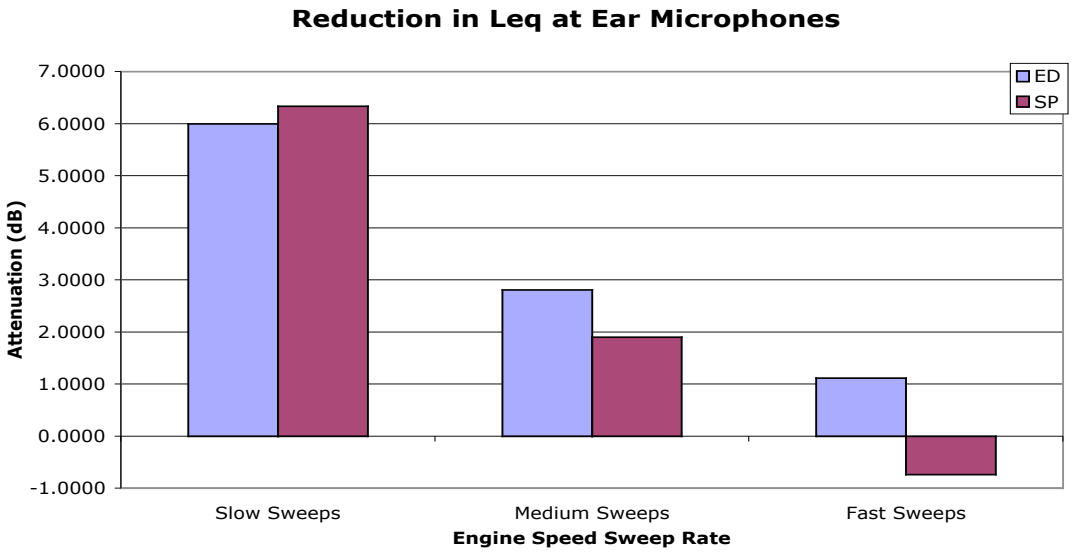

Figure 6.24 ANC system reduction of L_{eq} at the ear microphones. These results were obtained with recorded tractor noise as the excitation signal and the system operating at 2 kHz with 300-tap SysID filters.

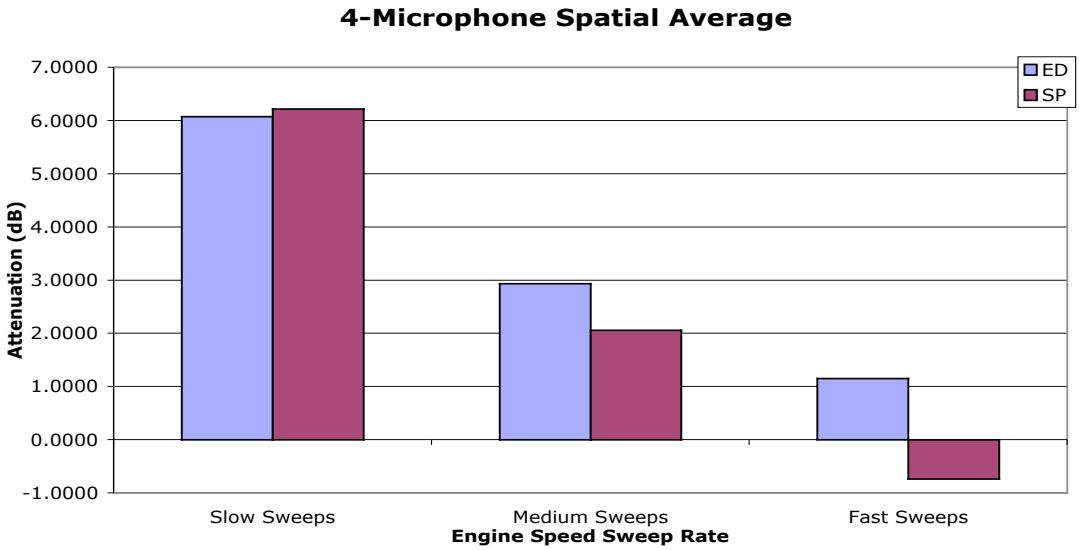

Figure 6.25 ANC system reduction of spatially averaged L_{eq}. These results were obtained with recorded tractor noise as the excitation signal and the system operating at 2 kHz with 300-tap SysID filters.

As shown in Figure 6.26, both ED and SP control provided significant levels of attenuation throughout the range of the engine firing frequency of the tractor. The spectra displayed in Figure 6.26 represent the slowest recorded sweeps through the

tractor's range of engine speeds. Figures 6.27 and 6.28 show similar spectra for the measurements using medium and fast sweeps, respectively. For the medium sweep rate, the spectra in Figure 6.27 show some frequency regions where the ED control produces higher net sound levels than the SP control, but fast sweep spectra in Figure 6.28 show the ED control outperforming the SP control in nearly all frequency regions.

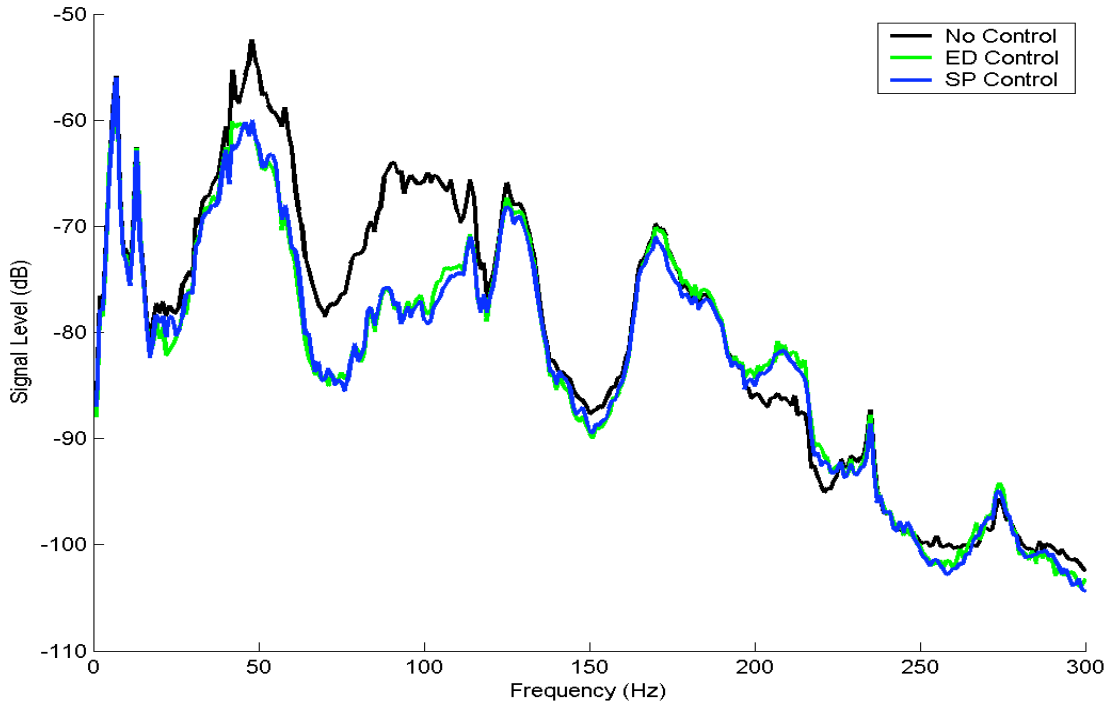

Figure 6.26 Time-averaged spectrum of recorded tractor noise excitation signal measured with and with out ANC by the left ear microphone, using slow engine speed sweeps.

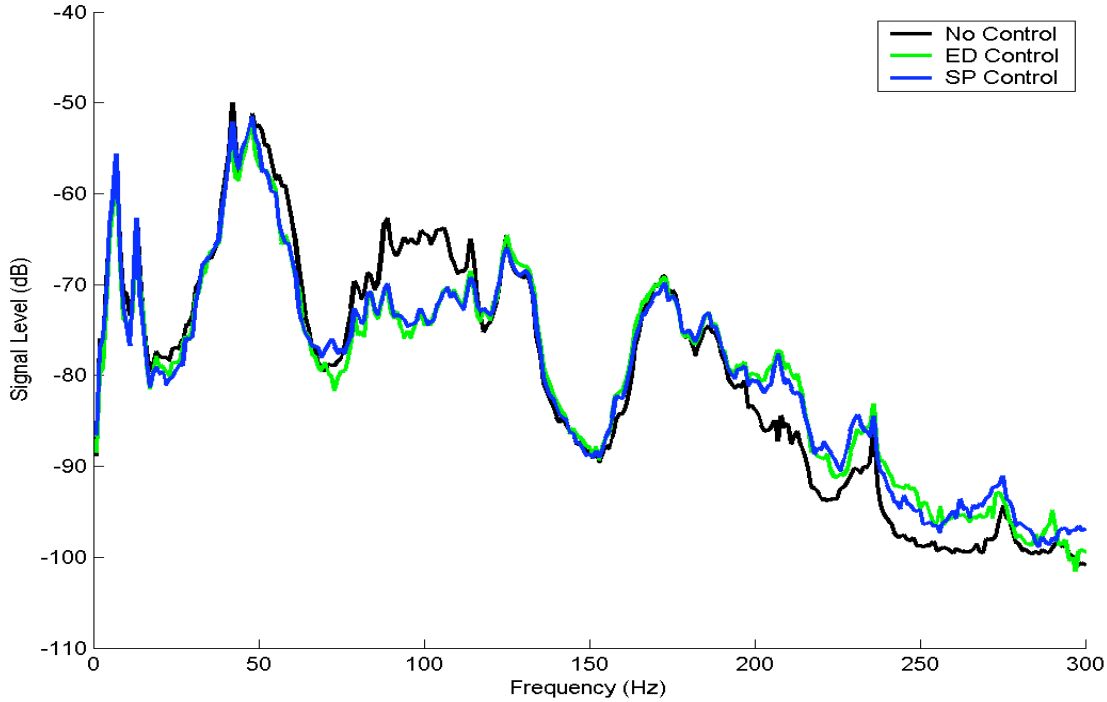

Figure 6.27 Time-averaged spectrum of recorded tractor noise excitation signal at the left ear microphone, using medium engine speed sweeps.

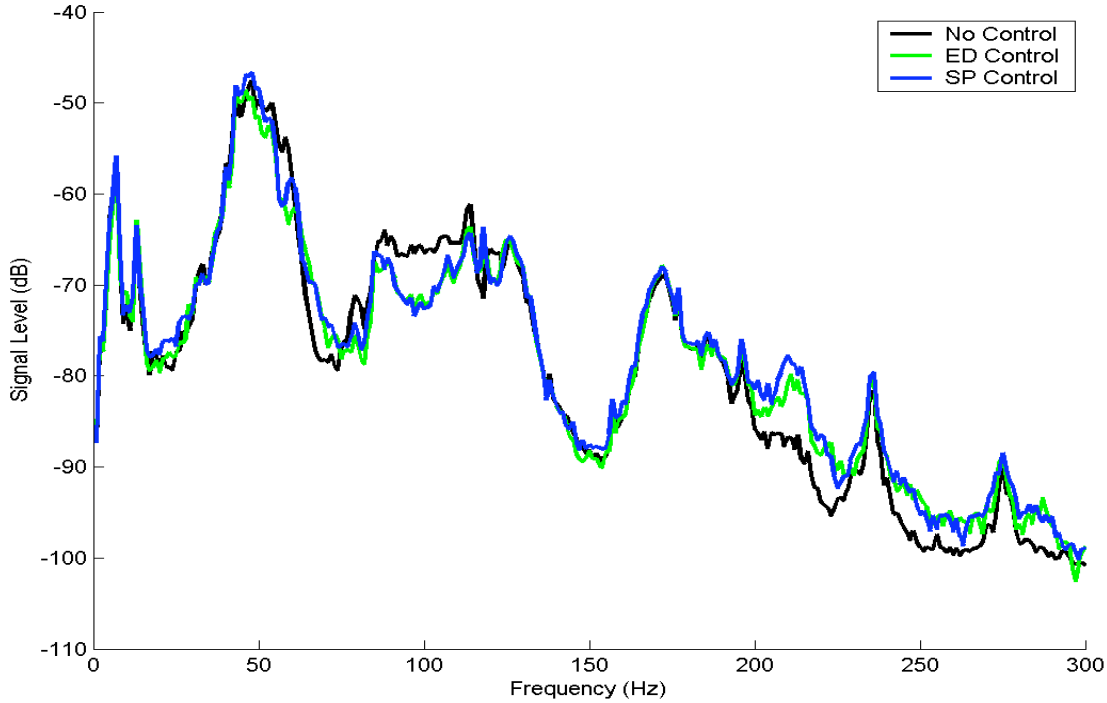

Figure 6.28 Time-averaged spectrum of recorded tractor noise excitation signal at the left ear microphone, using fast engine speed sweeps.

CHAPTER 7

CONCLUSIONS

An active noise control system, which minimizes acoustic energy density, has been successfully demonstrated in a mock tractor cabin. The system was shown to provide significant levels of attenuation when controlling tonal noise at fixed and varying frequencies. The ED-based algorithm often fails to provide better attenuation of static tonal noise than a similar control algorithm that minimizes squared pressure, especially at very low frequencies. However, ANC system performance measurements for static noise signals suggest that the tonal attenuation achieved by the ED-based control system is more uniform throughout the cab than that achieved by the SP-based control. Superior tonal attenuation at the error sensor does not necessarily imply better noise reduction at the tractor operator's ears. Also, more control channels and more powerful processors do not necessarily provide any appreciable benefit in terms of control performance.

When compared to SP-based control, ED control generally provides better attenuation of the equivalent sound level (L_{eq}) for tonal noise that is swept in frequency. ED control also provides attenuation near the tractor operator's ears, which is generally as good as, and often better than, the attenuation achieved by SP control. However, the additional component cost of an energy density sensor and the associated computational requirements may not justify the use of ED-based control over SP-based control in small tractor cabs with low modal density, especially when only low frequency engine tones are to be targeted by the ANC system. However, many real equipment cabins are larger than the mock cab used in this research, and may benefit more from ED based control. Additional advantages to ED control may also arise when controlling higher frequency

tones, such as second or third order engine firing frequencies.

The main objectives of this research—to demonstrate the successful operation of the active minimization of acoustic ED in a mock tractor cab and investigate its performance with static and dynamic noise signals—have been achieved. This work has also provided some additional understanding of the impact of the SysID filters and DSP capabilities on the ED-based control system, as well as a comparison of the relative performance of ED and SP-based control systems using one and two control channels.

7.1 Recommendations for Future Research

The research discussed in this thesis assumed that fixed SysID filter coefficients would allow the system to adapt more quickly to changes in the reference signal and therefore, the noise to be targeted. However, no effort was made to quantify the tracking speed of the control system when using online system identification rather than the fixed filter coefficients obtained via offline SysID. Experiments could be conducted to investigate this issue and perhaps some type of hybrid system could be developed in which the control system would begin operation with a fixed set of SysID coefficients available at run time, but include the ability to adapt to gradual or sudden changes in the secondary path. Additionally, for a similar ANC system to be employed in a real tractor, the actual cab in which it would be installed would have to be investigated to obtain the proper SysID filter lengths for optimal control performance.

The issue of maintaining a proper set of SysID models is one of maintaining stability of the control algorithm. In a commercial setting, in an actual tractor, it would be desirable to have a very robust control system. The goal is to reduce the amount of noise in the cab rather than increase it, so some sort of automatic reset or other safety

measures should be developed for such an application of ANC to prevent the equipment operator from being exposed to even higher sound levels in the event that the control algorithm does become unstable.

Time constraints did not allow for the investigation of including second and third harmonics of the targeted tonal noise in the ANC performance measurements prior to the writing of this thesis. Although the dominant tone in many tractor cabs is the engine firing frequency, harmonics of the engine firing frequency often make a significant contribution to the overall sound level, as well. Targeting these additional tones is recommended for future investigation of this active noise control system.

The ED ANC system has been shown to provide essentially global control of the fundamental engine firing frequency over the range of typical engine speeds. Despite the issues yet to be explored and challenges yet to be faced in the implementation of such an ANC system in real tractor cabins, this research provides evidence that an energy based control system can improve the working environment of equipment operators.

REFERENCES

1. P. Lueg, “Process of Silencing Sound Oscillations” (U.S. Patent No. 2,043,416, 1936).
2. H. F. Olsen and E. G. May, “Electronic Sound Absorber,” J. Acoust. Soc. Am. 25, 1130-1136 (1953).
3. Y. Peng, A. Sasao, and S. Shibusawa, “Active noise control in proximity of a tractor operator’s head,” Trans. ASAE, 44, 447-455 (2001).
4. E. Carletti, D. Stanzial, and I. Vecchi, “Application of the active noise cancellation technique to earth-moving machines,” Proc. Noise-93, St. Petersburg, Russia, May 31 – June 3, 1993, pp. 141-146.
5. E. Carletti and I. Vecchi, “Reduction of noise inside cabs of earth-moving machines by active noise cancellation technique,” Proc. Inter-Noise 94, Yokohama, Japan, Aug. 29-31, 1994, pp. 1417-1420.
6. E. Carletti, G. Miccoli, and I. Vecchi, “Earth-moving machine cab enclosed sound field active control simulation,” Proc. Inter-Noise 96, Liverpool, U.K., July 30 - Aug. 2, 1996, pp. 1183-1186.
7. J. W. Parkins, S. D. Sommerfeldt, and J. Tichy, “Narrowband and broadband active control in an enclosure using the acoustic energy density,” J. Acoust. Soc. Am. 108, 192-203 (2000).
8. S. D. Sommerfeldt and P. J. Nashif, "An adaptive filtered-*x* algorithm for energy based active control," J. Acoust. Soc. Am. 96, 300-306 (1994).
9. J. W. Parkins, S. D. Sommerfeldt, and J. Tichy, “Error analysis of a practical energy density sensor,” J. Acoust. Soc. Am. 108, 211-222 (2000).

10. J. W. Parkins, J. Tichy, and S. D. Sommerfeldt, "A comparison of two active control methods through an investigation of node structures," Proc. Active 99, Ft. Lauderdale, FL, Dec. 2-4, 1999, pp. 729-740.

11. G. W. Elko, ''An acoustic vector-field probe with calculable obstacle bias,'' Proc. Noise-Con 91, July, 1991, pp. 525–532.

12. L. L. Locey and S. D. Sommerfeldt, "Analysis and comparison of three energy density probe designs," J. Acoust. Soc. Am. 114, 2443 (2003).

13. P. A. Nelson and S. J. Elliott, *Active Control of Sound*, Academic Press, London, 1992.

14. C. H. Hansen and S. D. Snyder, *Active Control of Noise and Vibration*, E & FN SPON, London, 1997.

15. M. H. Hayes, *Statistical Digital Signal Processing and Modeling*, Wiley & Sons, New York, 1996.

16. B. Widrow and S. D. Stearns, *Adaptive Signal Processing*, Prentice-Hall, Englewood Cliffs, NJ, 1985.

17. S. M. Kuo and D. R. Morgan, *Active Noise Control Systems: Algorithms and DSP Implementations*, Wiley & Sons, New York, 1996.

18. S. D. Snyder, "Active control—a bigger microprocessor is not always enough," Noise Control Eng. J. 49, 21-29 (2001).